Diagnostics, Control and Performance Parameters for the BELLA High Repetition Rate Petawatt Class Laser

Kei Nakamura, *Member, IEEE,* Hann-Shin Mao, Anthony J. Gonsalves, *Member, IEEE,* Henri Vincenti, Daniel E. Mittelberger, Joost Daniels, Arturo Magana, Csaba Toth, and Wim P. Leemans, *Fellow, IEEE*

***Abstract*—A laser system producing controllable and stable pulses with high-power and ultrashort duration at high repetition rate is a key component of a high energy laser-plasma accelerator (LPA). Precise characterization and control of laser properties are essential to understanding laser-plasma interactions required to build a 10 GeV class LPA. This paper discusses the diagnostics, control and performance parameters of a 1 Hz, 1 petawatt (PW) class laser at the Berkeley Lab Laser Accelerator (BELLA) facility. The BELLA PW laser provided up to 46 J on target with a 1% level energy fluctuation and 1.3 μrad pointing stability. The spatial profile was measured and optimized by using a camera, wave front sensor, and deformable mirror (ILAO system). The focus waist was measured to be $r_0 = 53$ μm and a fraction of energy within the circular area defined by the first minimum of the diffraction pattern ($r = 67$ μm) was 0.75. The temporal profile was controlled via the angle of incidence on a stretcher and a compressor, as well as an acousto-optic programmable dispersive filter (DAZZLER). The temporal pulse shape was measured to be about 33 fs in full width at half maximum (WIZZLER and GRENOUILLE diagnostics). In order to accurately evaluate peak intensity, the energy-normalized peak fluence and energy-normalized peak power were analyzed for the measured spatial and temporal mode profiles, and were found to be 15 kJ/(cm^2 J) with 6% fluctuation (standard deviation) and 25 TW/J with 5% fluctuation for 46 J on-target energy, respectively. This yielded a peak power of 1.2 PW and a peak intensity of 17×10^{18} W/cm^2 with 8% fluctuation. A method to model the pulse shape for arbitrary compressor grating distance with high accuracy was developed. The pulse contrast above the amplified spontaneous emission pedestal was measured by SEQUOIA and found to be better than 10^9. The first order spatiotemporal couplings (STCs) were measured with GRENOUILLE, and a simulation of the pulse's evolution at the vicinity of the target was presented. A maximum pulse front tilt angle of less than 7 mrad was achieved. The reduction of the peak power caused by the first order STCs was estimated to be less than 1%. The capabilities described in the paper are essential for generation of high quality electron beams.**

Manuscript received March 14, 2017; revised April 28, 2017; accepted May 4, 2017. Date of publication Month Day, 2017.

This work was supported by the Director, Office of Science, Office of High Energy Physics of the U.S. Department of Energy under Contract No. DE-AC02-05CH11231. D. E. Mittelberger was supported by the National Science Foundation.

K. Nakamura, H.-S. Mao, A. J. Gonsalves, H. Vincenti, D. E. Mittelberger, J. Daniels, A. Magana, C. Toth and W. P. Leemans are with the Lawrence Berkeley National Laboratory, Berkeley, CA 94720, USA. E-mail: KNakamura@lbl.gov, WPLeemans@lbl.gov.

H. Vincenti is also with Lasers, Interactions and Dynamics Laboratory, CEA Saclay, France.

J. Daniels is also with Eindhoven University of Technology, Eindhoven, The Netherlands.

D. E. Mittelberger and W. P Leemans are also with University of California Berkeley, Berkeley 94720 CA.

***Index Terms*—Chirped-pulse amplification, Ti:Sapphire lasers, Adaptive optics, Spatiotemporal couplings, Laser-plasma accelerators.**

I. Introduction

LASER plasma accelerators (LPAs) [1] have the potential to provide tools to accelerator science with characteristics that have been unattainable through conventional accelerator technologies. Their high accelerating fields can provide small footprint, cost-effective electron accelerators for high energy physics [2], [3], and their short characteristic plasma wavelength naturally provides femtosecond electron beams, useful for ultrafast science applications [4]–[6].

The technology of LPA has advanced due to the progress in CPA (chirped pulse amplification) laser technologies [7]. Ti:sapphire lasers can routinely provide pulses with 10s of fs duration, realizing high peak power with relatively low pulse energy. This gives an advantage in the repetition rate compared to glass medium based high power laser systems. High repetition rate systems allow a wider range of parameter searches and have contributed to the rapid progress in the field. Their ultrashort pulses can match the plasma wavelength, enabling 100 MeV class quasi-monoenergetic electron beam generation with 10 TW class lasers [8]–[10]. The availability of high peak power lasers has led to many facilities generating GeV-level electron beams [11]–[16].

In order to realize a 10 GeV class LPA, designs have been developed at Lawrence Berkeley National Laboratory (LBNL) that utilize meter-scale accelerator structures powered by a petawatt (PW) class laser system. The design led to the formation of the BELLA (BErkeley Lab Laser Accelerator) project [17]. In 2012, the world's first commercial PW laser system was acquired from THALES [18] and commissioned at the LBNL BELLA facility to explore the development of a 10-GeV-class LPA and its associated laser-plasma interaction physics. Among the active PW class laser systems in the world [19]–[25], the BELLA PW laser operates with the highest average power, 46 W, and has currently produced up to 4.2 GeV electron beams [26], [27] using 9 cm-long preformed plasma channels [28], [29].

Precise characterization and control of the laser properties is critical to develop a 10-GeV-class LPA. For example, in the highly nonlinear regime [30], small variations in input laser peak intensity resulted in large output fluctuations [9]. For a PW laser pulse, a percent level prepulse might generate

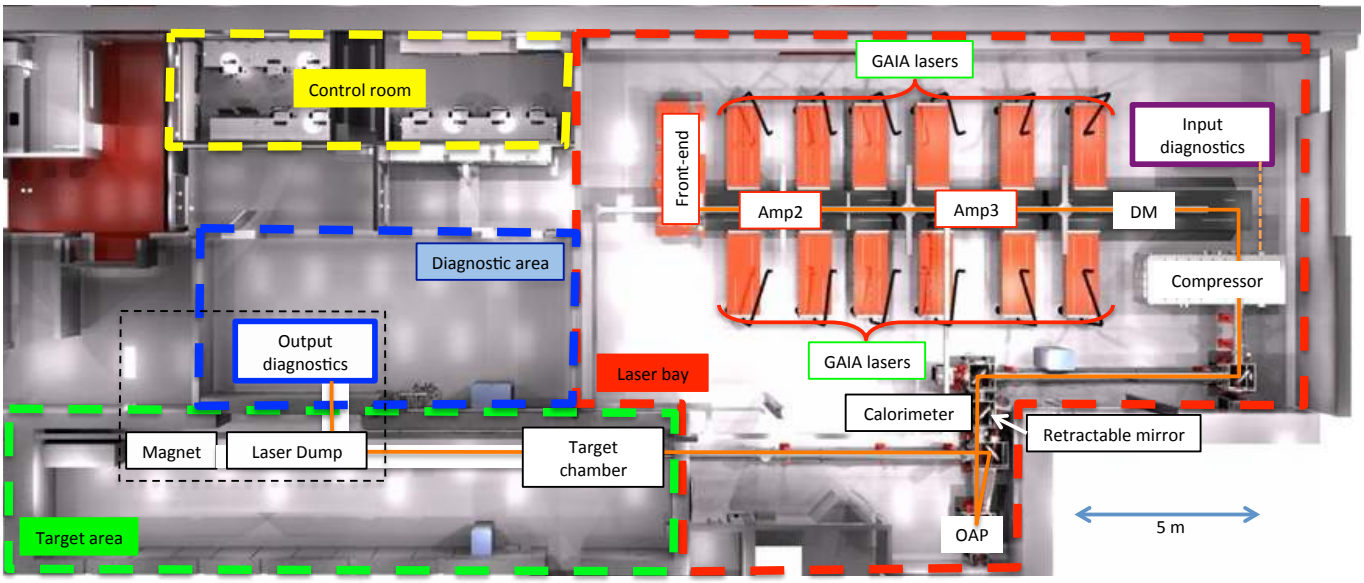

Fig. 1. Floor map of the BELLA PW facility. The front-end included everything from the oscillator to the first multi-pass amplifier (Amp1), as indicated in Fig. 2. The power supplies of the pump lasers were located in the room above the laser bay (not shown) for better environmental temperature stability. A deformable mirror (DM) was located between the Amp3 and the compressor. The laser propagated in air down to the compressor input, and entered the vacuum system at the compressor toward the target chamber and diagnostics. The laser pulses were focused using a 13.5 m focal length off-axis paraboloid (OAP). At the laser beam dump, a small percentage of the beam was sampled and sent to the output diagnostic. This region is detailed in Fig. 6. At the compressor output, a small percentage of the beam was also sampled and sent to the input diagnostics.

sizable wakefield before the arrival of the main pulse. Detailed knowledge of the laser's transverse mode properties are crucial to understanding the laser propagation and the generation of high energy electron beams [27], [31]. High quality spatial mode and stable beam pointing are essential for structured targets such as a preformed plasma channel. The higher peak power laser requires higher quality in spatial and temporal contrast. Spatiotemporal couplings (STCs) can significantly lower the pulse peak intensity if not properly taken care of [32] and can affect LPA performance [33], [34]. There have been only a couple of studies published on how STCs affect LPA performance. It is considered to be critical to have capabilities of diagnosing and controlling STCs toward realization of a 10 GeV class LPA.

In this paper, diagnostics, control and performance parameters for the BELLA PW laser system are discussed. Sec. II gives a system overview, where energy and pointing stabilities are also discussed. Diagnostics and control for the laser spatial mode are discussed in Sec. III, for the temporal mode in Sec. IV, and for the spatiotemporal couplings in Sec. V. Lastly, summary and conclusions are provided in Sec. VI.

II. System Overview

THE world's first 1 Hz repetition rate 1 PW laser was acquired from THALES and installed at the BELLA PW facility in 2012, and since then, has gone through several modifications and upgrades. The floor map of the BELLA PW facility is shown in Fig. 1. It consists of a control room and three experimental areas, namely the laser bay, the target area, and the diagnostic area. Note that the components purchased from THALES included the laser amplifiers, the compressor and the input diagnostics illustrated in Fig. 1. Everything following the compressor output, which include the beam transport line, target chamber, and output diagnostics, were built by LBNL. The following section describes the facility, the laser amplification stages, and the key components such as the stretcher and compressor systems. Additionally, the energy and pointing stabilities are presented.

The system is based on a double-CPA architecture of Ti:Sapphire amplifiers, where an XPW (cross-polarized wave) contrast enhancement system [35] (referred to as XPW hereinafter) is installed in between two CPA systems. Figure 2 illustrates a schematic diagram of the system. The first CPA (CPA1) consists of an oscillator, a stretcher, a regenerative amplifier (RA), and an optical compressor. It is capable of producing pulses with 40 nm bandwidth and 700 μJ at a repetition rate 1 kHz. By tuning the bandwidth of the Vitara-T oscillator (Coherent [36]), the CPA1 output bandwidth is arranged to be 30 nm in full width at half maximum (FWHM), and matches the bandwidth of the XPW output beam to the bandwidth of the CPA2 system, minimizing degradation of the contrast of the pulse [37]. Note that with a flat spectral-phase input pulse to the XPW, the output spectrum is expected to have a broader bandwidth by a factor of $\sqrt{3}$ [38].

The CPA1 output temporal profile was measured by a WIZZLER 800 (Fastlite [39]), and is shown in Fig. 3. The bandwidth was 30 nm (FWHM) and spectral phase was flat within 0.5 radian, which resulted in a 45 fs FWHM pulse width. The vertical axis of the Fig. 3 (b) is the instantaneous power normalized by the total energy, $P_E(t)$ [TW/J], showing the power for a pulse with 1 J of energy. In this manner, one can see the peak power $P_0 = E_L P_E(0)$ more precisely including the effect of the femtosecond scale pre and post pulses compared to simply evaluating power by pulse energy

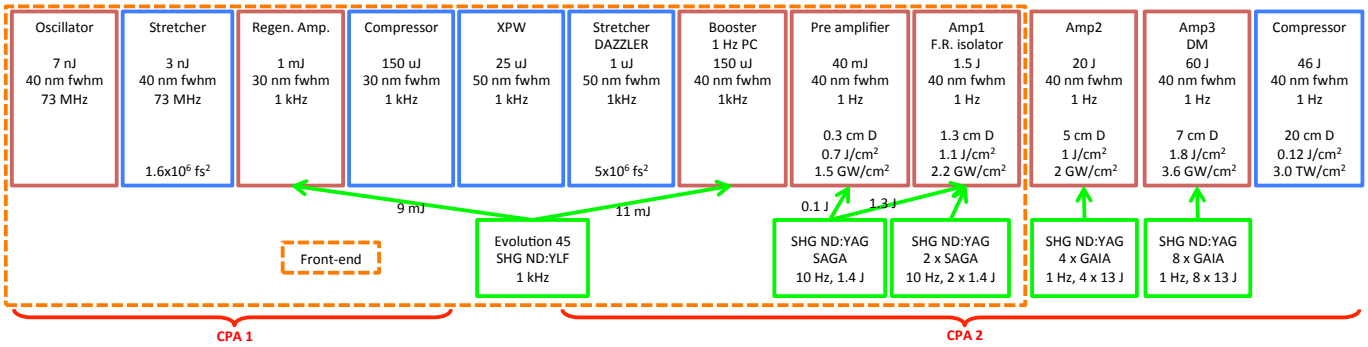

Fig. 2. Components of the BELLA PW laser system. The numbers in the boxes are for output beam properties of each component, except the designed group velocity dispersion for stretchers. All the laser components were purchased from THALES except the Oscillator (VITARA-T, Coherent) and 1 kHz pump laser (Evolution 45, Coherent). An acousto-optic programmable dispersive filter (DAZZLER, Fastlite) was placed after the second stretcher, a 1 Hz Pockels Cell (PC) optical shutter at the Booster output, a large-diameter Faraday Rotation isolator (F.R. isolator) at the Amp1 output, and a deformable mirror (DM) at the Amp3 output.

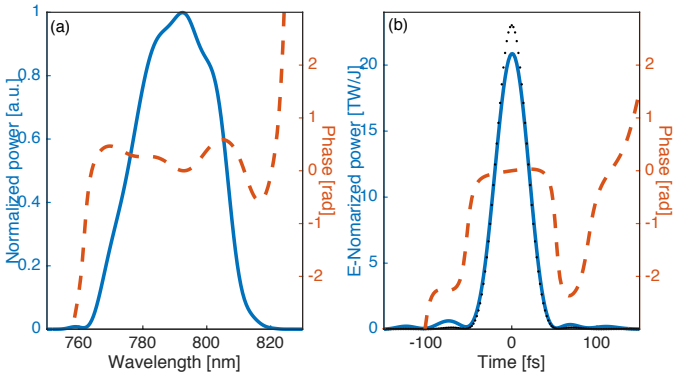

Fig. 3. The CPA1 output pulse in (a) spectral domain and (b) time domain. Shown by solid blue lines are the power, and dashed orange lines are the phase. The central wavelength was 788 nm and the bandwidth was 30 nm FWHM. The pulse length was 45 fs FWHM, and the energy-normalized peak power was 21 TW/J. The black doted line in (b) shows the temporal profile for a FL pulse (flat spectral phase).

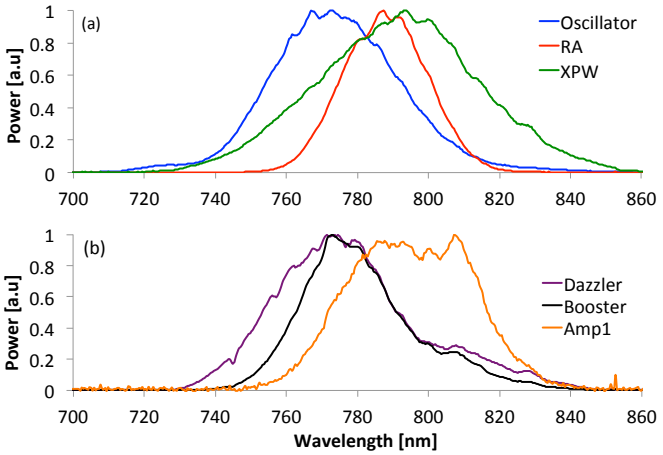

Fig. 4. Typical output optical spectra for (a): Oscillator, RA and XPW, (b): DAZZLER, Booster and Amp1.

divided by pulse length. Here, E_L is the laser pulse energy. The temporal profile for the case of a Fourier-limited (FL) pulse (flat spectral phase) is shown by the black dots. The peak power of the measured pulse was found to be 90% of the FL pulse. This number is an indicator of the quality of the spectral phase, and discussed in more detail at Sec. IV-B.

The CPA1 beam output energy is attenuated to 150 μJ/pulse to avoid white light generation at the XPW. The XPW utilizes two BaF_2 crystals [40] to enhance efficiency, and these crystals are wedged to avoid multiple reflections on-axis. The output energy is typically 25 μJ/pulse with 50 nm FWHM bandwidth. The energy efficiency (17%) and the spectral broadening (x1.7) indicate that the quality of input pulse temporal mode is nearly optimized [41]. The pulse contrast is discussed in the Sec. IV. Figure 4 (a) shows typical optical spectra for the oscillator, RA, and XPW output, where significant redshift at the RA can be seen. The central wavelength of the oscillator is tuned towards shorter wavelength to pre-compensate spectral redshift in the subsequent amplifiers. The spectrum broadening at the XPW can also be seen from Fig. 4 (a).

The XPW output is then stretched and sent to an acousto-optic programmable dispersive filter, DAZZLER HR800 with a 50 W RF amplifier (Fastlite), to control the spectral phase distribution. The spectral phase tuning is discussed in Sec. IV-B. A Pockels cell (PC) based pulse cleaner is placed after the booster amplifier together with a mechanical shutter to reduce the repetition rate to 1 Hz. The laser pulses pass through 4 more multi-pass amplifiers to eventually reach 60 J/pulse. The energy for amplified and pump beams are shown in Fig. 2.

The DAZZLER is also capable of modulating the spectral amplitude to compensate against spectral redshift in subsequent multi-pass amplifiers. Shown in Fig. 4 (b) is the typical output optical spectrum at the DAZZLER, the booster amplifier, and the amplifier 1 (Amp1) output. The spectral amplitude is typically modulated by the DAZZLER with a 65% notch at 800 nm with 52 nm width (applied in its native software) for the specific spectra shown in Fig. 4 (b). One can see that the spectral intensity modulation causes the spectrum to be skewed toward shorter wavelength, but after Amp1 the spectrum is relatively symmetric. The amount of the spectral redshift and gain narrowing depends on the pump energy at amplifier 2 (Amp2) and amplifier 3 (Amp3). The optical spectrum at the target is tuned by changing the spectral

amplitude modulation parameters of the DAZZLER for each pump energy to ensure sufficient bandwidth.

All the Ti:Sapphire amplifiers described here utilize room-temperature water cooling. The temperature of the crystals reaches equilibrium state within an hour. The pump energy for the front-end amplifiers is fixed such that the output laser pulse energy and other parameters such as divergence are fixed. The pump energy for Amp2 and Amp3 amplifier stages is varied to deliver a specific on-target energy. This operation results in varying Amp3 output laser beam divergence depending on the delivered energy, and requires devices that monitor and adjust the beam properties. Therefore, a deformable mirror (DM) was installed in between Amp3 and the CPA2 compressor and a wavefront sensor at the input diagnostics area, shown in Fig. 1.

The mirror right after the final grating at the CPA2 compressor leaks 1% of the beam, which is sent to the input diagnostics area. Here, a part of the beam is sent to a wavefront sensor (HASO 32, Imagine Optic [42]), imaging the DM plane. The input diagnostic also include cameras to monitor near and far field beam profiles as well as a single-shot energy detector (QE12, Gentec-EO [43]). The same spectral amplitude profile as that of the main beam line is maintained by a special spectral filter designed for this beam line. Accumulated B-integral, $B = 2\pi/\lambda \int n_2 I(z) dz$, for this area was estimated to be $B(2\text{ J}) \sim 3.4$ and $B(46\text{ J}) \sim 9.5$ for each on-target energy. Due to this high accumulated B-integral for high energy operation, detailed study for laser beam properties were mainly performed at the output diagnostic area. The spatial mode tuning using the ILAO (Intense Laser Adaptive Optics) system (a package of the DM, wavefront sensor, and software from Imagine Optic) is detailed in Sec. III.

The output energy for the pre-amplifier, Amp1, Amp2 and Amp3 are always monitored by sampling a fraction of the beam with uncoated thin wedges and sending it to single-shot energy meters (QE12). Those energy meters are cross-calibrated by measuring the main laser power with a larger format energy meter (QE95, Gentec-EO). The on-target laser energy is measured by using a large diameter calorimeter (CM310, Gentec-EO) located between the CPA2 compressor and an off-axis paraboloid (OAP) as indicated in Fig. 1. By inserting the retractable mirror, the laser can be sent to the calorimeter. Note that the calorimeter is not a single-shot diagnostic but measures average power. By comparing the calorimeter measurements and the Amp3 energy measurements, the throughput energy efficiency from Amp3 output to the target can be evaluated. Single-shot on-target energy is calculated from the Amp3 output measurements. The throughput efficiency of the CPA2 compressor was measured to be about 80%. Figure. 5 shows the measured Amp3 output energy for 1800 consecutive shots, where average energy was 55.5 J with a standard deviation of 0.3 J (0.54%).

Damages in optics are common issue for high power laser systems. As of April, 2017, the BELLA PW laser has been free from any recurring damage issue for optics before the 2nd compressor since its commissioning in 2012. Estimated beam fluence and intensity for 1 Hz amplifiers are shown in Fig. 2. The laser beam fluence has been kept under 2 J/cm^2 to avoid damages. For optics further downstream, gratings in the optical

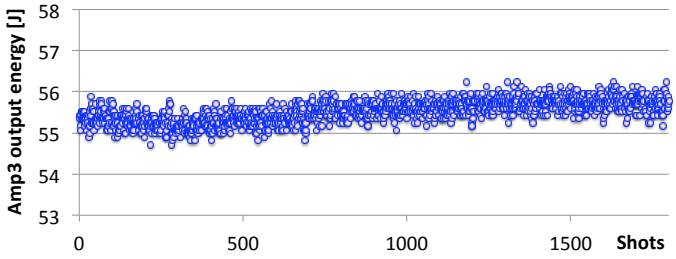

Fig. 5. Amp3 output energy for 1800 consecutive shots. Average energy was 55.5 J and standard deviation was 0.3 J.

compressor are known to have the lowest damage threshold in the system. The fluence on the grating was arranged to be about 0.1 J/cm^2. Although a development of white smudge-like profile that resembles beam near-field profile at the last contact surface has been visible, no significant reduction in the compressor efficiency has been observed yet. This development is certainly a concern, and a dedicated camera to monitor the evolution of these features has been implemented. Optical coatings for other steering optics after compression including OAP are also regularly inspected, and other than minor crazing lines of the coatings and occasional minimal darkening, no significant deterioration has been observed yet.

The laser pulses are focused using the 13.5 m focal length OAP to a focal spot size of $w_0 \simeq 53$ μm, where the transverse (radial) electric field of a pulse is defined as $E(r) \propto \exp\left[-(r/w_0)^2\right]$. The laser vacuum focus is located at the upstream side of the target chamber shown in Fig. 1, where a target for laser-plasma acceleration experiments resides.

The post-interaction laser pulses are then sent to the laser dump/output diagnostic area. Schematics of the area are shown in Fig. 6. A fraction of the laser pulse is first sampled by an uncoated wedge with a 25.4 mm diameter hole to allow passage of the accelerated electron beam and sampling of the laser pulse. The majority of the laser pulse is absorbed by another multi-shot averaging calorimeter (CM310, Gentec-EO), with a 25.4 mm diameter hole for the electron beam. The remaining center portion of the laser pulses is separated from the electron beams by a gold-coated Mylar foil. Electron beam diagnostics are described in other publications [26], [27], [44]–[46].

The output diagnostics include an all-reflective aberration-free telescope which relayed images of the laser-plasma interaction point in the target chamber to the output diagnostic area. Note that many optics are omitted in Fig. 6 for simplification. The set of relay optics includes three uncoated wedges (two of them are in-vacuum) to attenuate laser pulse energy by a factor of 3.7×10^{-5}. A camera on a translation stage (mode imager in Fig. 6) images the beam over a range of 40 cm around the vacuum laser focus. The near-field camera (see Fig. 6 for location) is used to record near-field mode profile, and an optical spectrometer (C10083CAH, Hamamatsu photonics [47]) is placed at the same area. Temporal profile diagnostics, namely GRENOUILLE 8-20-USB (Swamp optics [48]), WIZZLER, and SEQUOIA 800 (Amplitude Technologies [49]) reside in the same area, where a fraction of the beam is sampled and

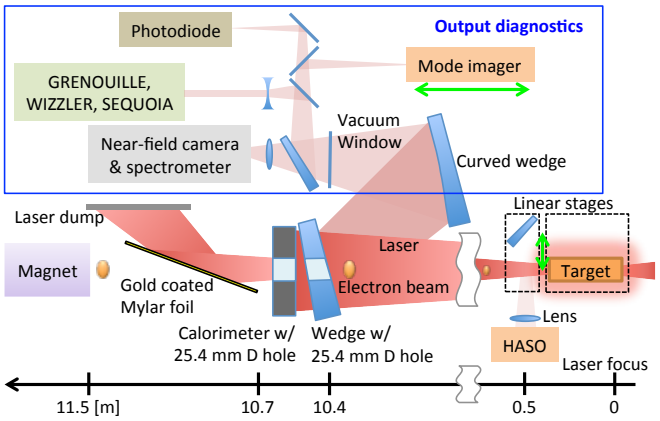

Fig. 6. Schematic for the target chamber, laser beam dump, and output diagnostic area. See manuscript for details. Note that the image is not to scale and many optics are omitted for simplification. The distances illustrate the relative spacing between beamline elements. The target chamber held retractable stages for both the LPA target and a wedge for wavefront measurements (see Sec. III for wavefront measurements).

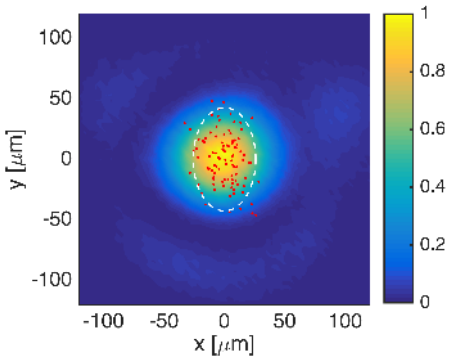

Fig. 7. Typical vacuum focus mode profile measured by the mode imager. Shown by red dots are 100 consecutive beam centroids, and by white dashed line is 2σ (95%) ellipsoid. (The horizontal and vertical angular pointing fluctuations of the laser pulses were measured to be $\sigma_{x'}$ =0.96 μrad and $\sigma_{y'}$ =1.58 μrad, respectively. The color map shows normalized fluence.

collimated. A fraction of beam is also focused to a photodiode (DET10A, Thorlabs [50]) to monitor nano-second-scale temporal profile of pulses. Details of the temporal domain diagnostics are described in Sec. IV.

Pointing stability of the laser is one of the most critical parameters for a high power laser system to drive LPAs, especially when structural targets, such as a capillary discharge plasma channel, are used. The pointing stability was measured using the mode imager at the output diagnostics. Figure 7 shows a typical mode profile by color map, and 100 consecutive beam centroids by red dots. Standard deviations for the horizontal and vertical pointing angles were measured to be $\sigma_{x'}$ =0.96 μrad and $\sigma_{y'}$ =1.58 μrad, and maximum deviations were $x'_{max} = 2.45$ μrad and $y'_{max} = 3.56$ μrad, respectively. Here, $x' = dx/dz$ and $y' = dy/dz$, respectively. The small laser pointing fluctuation allows the use of preformed plasma channels as targets.

In summary, the BELLA PW laser is a double-CPA based, PW class, Ti:Sapphire amplifier system. High quality 1 kHz repetition rate 45 fs (30 nm FWHM bandwidth) laser pulses with 150 μJ/pulse are provided by CPA1, and contrast is improved with XPW. The CPA2 amplifiers and relevant diagnostics were discussed. The excellent on-target energy stability (0.54% standard deviation) and pointing stability (0.96 μrad horizontally and 1.58 μrad vertically) were demonstrated.

III. Spatial Domain

THE BELLA PW laser has produced up to 4.2 GeV electron beams using preformed plasma channels. This capillary discharge waveguide extended the interaction length between the high intensity laser and the plasma, producing higher electron beam energy than simple gas-jet targets. Maintaining an excellent spatial mode is of paramount importance in order to properly couple the beam into the plasma channel. A study indicated that the halo of the focus can affect LPA performance significantly [51]. The >40 J pulses can have an appreciable amount of energy in the tails, which could potentially damage the structure and disrupt the waveguide.

The final two amplifier crystals measure 8 cm and 12 cm in diameter. Although the crystals are liquid cooled with forced flow, they are still susceptible to thermal lensing which introduces aberrations in the beam. As discussed in Sec. II, this effect could vary significantly depending on how much laser energy is deposited and/or extracted by the pump and main lasers. The location of the laser focus with respect to the plasma channel entrance is one of the critical parameters for achieving proper laser guiding. To compensate for the lensing, along with higher order aberrations inherent to the system and beam profile, a laser beam spatial mode correction is performed using a DM. This mirror was specifically designed for high-power laser applications [52].

In this section, the implementation of an adaptive optics system on the BELLA PW laser system is discussed along with the components and their benefits to PW-class lasers [53]. The efforts to deliver the highest possible spatial quality are explained along with operational precautions used as power was increased during experiments. Methods to evaluate the peak intensity accurately and to discuss spatial mode quality are discussed as well as performance parameters for the spatial domain.

A. ILAO Implementation and Operation

Spatial mode correction systems using a wavefront sensor and a DM have been employed in many high power laser facilities [21]–[23], [54]. Implemented in the BELLA PW laser system is the ILAO system, which has been developed by Imagine Optic and consisted of a Shack-Hartmann wavefront sensor (HASO) and DM for optical control [52]. The wavefront sensor is located at the input diagnostic and the DM between Amp3 and the CPA2 compressor as described in Sec. II and Fig. 1. The deformable mirror was installed before the compressor chamber to ensure the laser intensity was well below the damage threshold of the mirror coating.

The DM uses 52 mechanical pistons to shape the substrate. The motors for the pistons are turned off between movements, which passively holds the mirror shape without introducing

This article has been accepted for publication in a future issue of this journal, but has not been fully edited. Content may change prior to final publication. Citation information: DOI 10.1109/JQE.2017.2708601, IEEE Journal of Quantum Electronics

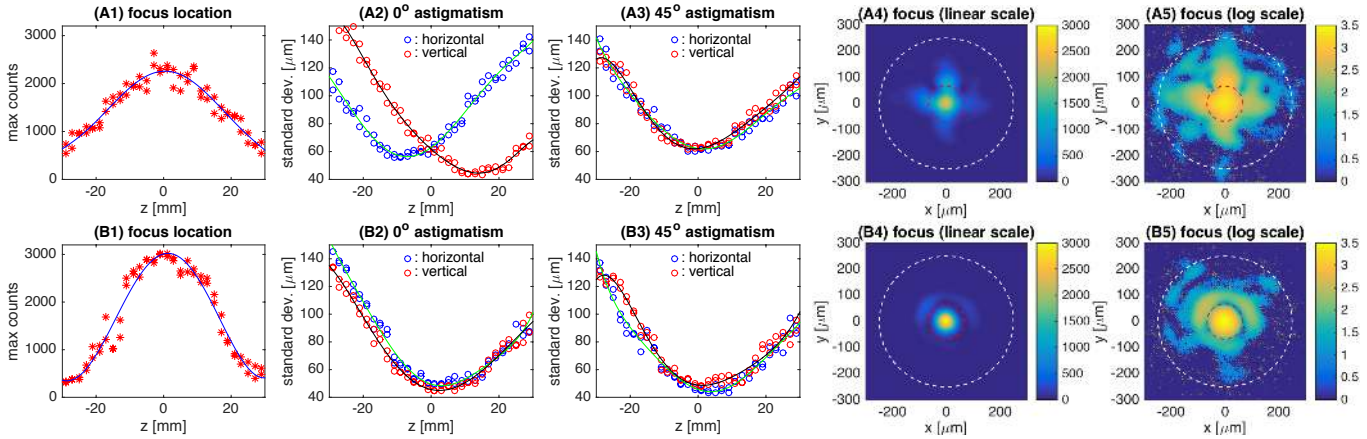

Fig. 8. Mode imager measurements before (A1-A5) and after (B1-B5) the open-loop procedure that is described in the manuscript. Prior to the measurements shown in (A1-A5), the on-target energy was increased from 29 J to 46 J by changing the pump energy on the Amp3. The peak fluence as a function of the beam propagation axis z is shown in (A1) and (B1) by the maximum counts on the camera, where $z = 0$ is the designed vacuum focus location. The horizontal and vertical standard deviations of the integrated beam profile as a function of z are shown in (A2) and (B2), which visualize 0 degree astigmatism. The same analysis for 45-degree rotated image was done and shown in (A3) and (B3) to visualize 45 degree astigmatism. The measured image at focus ($z = 0$) are shown in (A4) and (B4) with linear scale, and in (A5) and (B5) in log scale. Dashed red circles in (A4-5) (B4-5) indicate radius for the first minimum of the diffraction pattern ($r = 67$ μm), and a fraction of energy within the circle was measured to be 0.55 for (A4-5) and 0.75 for (B4-5), respectively.

thermal energy. This provides an advantage over piezo-based mirror technologies that require continuously applied power. In addition, mechanical pistons provide a wider range of motion than piezo-based mirror.

The disadvantage is that the motors have to go through a procedure that accounts for backlash in order to maintain the required precision. In practice, this manifests as the beam executing a swinging motion about ± 50 μrad while the mirror movement is occurring. This process was slow with respect to the repetition rate of the laser, 1 Hz. This precluded correction at higher laser energies in order to protect expensive optics such as the compressor gratings from local hotspots that may develop during correction. As a consequence, mirror corrections are only applied while the beam is blocked or when the beam energy is significantly below full energy ($<$2 J).

In order to determine the transfer function between mirror movements and the observed wavefront (called command matrix), the 52 pistons within the mirror are moved individually and the resultant wavefront for each piston move is recorded to obtain the so-called interaction matrix. The system then inverts this interaction matrix to obtain the command matrix, and actuator commands are decomposed into a series of up to 52 Zernike polynomials. Corrections to the Zernike aberrations could then be applied as a sequence of coefficients.

The optimization of the spatial mode begin by taking a measurement of the initial wavefront. The measured wavefront is decomposed into a series of Zernike coefficients, and the opposite Zernike coefficient values are applied to the DM through the obtained command matrix described in Sec. III-A. The correction typically requires iteration and the process can be repeated until the rms (root-mean-square) of the residual wavefront phase error, σ_Φ, is converged. It typically converges down to $\lambda_0 \sigma_\Phi / 2\pi \leq 40$ nm, where λ_0 is the laser central wavelength. This iterative "closed-loop" operation could be done automatically through the software. The quality of the correction depends on the stability of the beam and the accuracy of the command matrix.

This process provides pulses with flat wavefront phase at the wavefront sensor, but it does not necessarily provide pulses with optimum wavefront phase at the laser-plasma interaction point. After the beam is split, the main beam and the diagnosing beam goes through different optics accumulating different aberrations. This aberration difference is determined by measuring wavefronts simultaneously at the target and at the input diagnostic using a second wavefront sensor. The location of the second wavefront sensor is illustrated in Fig. 6 as HASO. A retractable wedge sends the laser pulse to the second wavefront sensor and a lens images the plane of the DM with the requisite magnification.

With the process described above, the wavefront at the interaction point can be optimized, and simultaneous measurement with the first wavefront sensor at the input diagnostics provides the aberration introduced between the two sensors. Since the second wavefront sensor can not be used with the target, this somewhat aberrated wavefront at the input diagnostic is used as the reference wavefront to provide optimum wavefront at the target during the laser-plasma interaction experiments.

During high-power operation, the closed-loop procedure described above is performed at $<$2 J on-target laser energy. For higher energies, the closed-loop operation is not performed to avoid potential damage to optics due to the "beam swinging". As laser energy increases, it has been empirically observed that aberrations introduced are dominated by 0° astigmatism, 45° astigmatism, and longitudinal focus shift. These could be measured by the mode imager from Fig. 6 which scans through focus. Corrections are then manually applied adjusting the Zernike coefficients for those three aberrations while the beam is blocked ("open-loop" operation).

Figure 8 shows an example of measurements of the focal region made by the mode imager before and after the open-loop correction. Shown in the first row (A1 - A5) are the mode imager measurements result just after the on-target energy was

increased from 29 J to 46 J. Note that the DM had been tuned to compensate for thermal loading of the crystals at 29 J operation. From the standard deviation of the integrated mode profile in horizontal and vertical axis as a function of longitudinal axis z shown in Fig. 8 (A2), one can see that the mode has significant astigmatism, about 21 mm focus location difference between the two axes.

The mode imager measurements result after the open-loop process is shown in Fig. 8 (B1-B5). By comparing (A1) and (B1), the peak fluence as a function of longitudinal axis, a significant improvement in peak fluence was achieved. Astigmatism (0 deg and 45 deg) was well corrected according to (B2) and (B3), and an overall mode quality improvement can be seen through comparison of the mode in both linear and log scale as shown in (A4), (A5), (B4) and (B5). The minimum possible step that could be obtained for the BELLA laser system was a 2 mm shift in focal location, which was about 20% of the Rayleigh length ($z_R = \pi w_0^2/\lambda_0 \sim 11$ mm). Based on a Gaussian fit to the focus shown in Fig. 8 (B4), the focus waist size was $w_{0x} = w_{0y} = 53$ μm.

B. Spatial Mode Quality

The Strehl ratio S is a commonly used measure to discuss quality of the focus [55], [56]. It can be approximated by using the rms wavefront phase error [57],

$$S \simeq \exp\left(-\sigma_\Phi^2\right). \quad (1)$$

After the closed loop operation described above, the wavefront typically converged to have $\sigma_\Phi \sim 0.3$, which gives $S = 0.9$. Note that the measured wavefront phase error is associated with the wavefront at the location of the DM, namely wavefront phase deviation from 0 at the near field. For a beam with Gaussian spatial profile, one may estimate the peak intensity of the pulse as $I_0 = 2SE_L P_E(0)/\pi w_0^2 = 23$ EW/cm^2 where $E_L = 46$ J, $P_E(0) = 25$ TW/J, $w_0 = 53$ μm and EW is Exawatt. Note that this estimate would be accurate only if the spatial amplitude profile has a Gaussian shape. The Strehl ratio addresses quality of the wavefront phase, but not of the amplitude profile.

In order to increase efficiency in the laser pulse amplification, flat-top or a super-Gaussian near field profile of the form of $I(r) \propto \exp\left[-2(r/w_n)^M\right]$ is commonly used for high power laser systems [22], where r is the distance from the beam center, w_n is the beam waist for near-field, and N determines the shape. For BELLA PW system, measurement of the near field profile showed $M \sim 10$, and found to have significant effects in the propagation in the plasma channel [26], [27]. Figure. 9 shows a corresponding near-field horizontal lineout for the beam shown in Fig. 8 (B). The blue solid curve shows measured profile, and red dashed line a super-Gaussian curve with $w_n = 71.5$ mm and $M = 10$. It was measured by the near-field camera that images the surface of the wedge with a hole, and therefore 25.4 mm diameter hole is visible (see Fig. 6 for location). Such a high-order near-field super-Gaussian profile gives a focal spot with a significant portion of energy outside of the main structure, even with a perfect wavefront phase at near field.

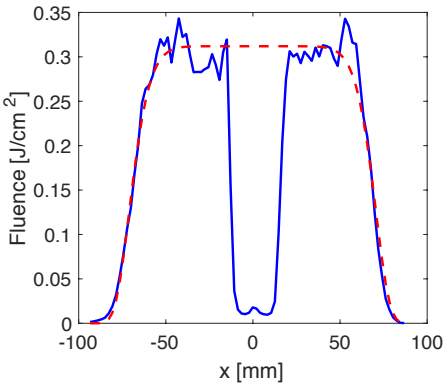

Fig. 9. Near-field horizontal lineout for the beam shown in Fig. 8 (B). The solid blue curve shows the measurement and the dashed red curve a fit to super-Gaussian shape with $w_n = 71.5$ mm and $M = 10$.

To discuss quality of the focus including this non-Gaussian near field effect, a fraction of energy within the first minimum of the diffraction pattern was evaluated. For the case shown in Fig. 8 (B), the first minimum was found at 67 μm (indicated by the red dashed circle), and a fraction of energy within $r = 67$ μm was 0.75. For a comparison, a fraction of energy within $r = 67$ μm for the case before the optimization, (A), was 0.55. This number gives intuitive understanding on how much energy is in the tails of the beam, and can be useful for comparing the quality of the spatial mode profile between different laser systems. Note that this measurement was limited by the dynamic range of the camera.

In order to estimate the peak intensity of the pulse accurately, it is convenient to evaluate energy-normalized fluence $F_E(r)$, that gives the fluence for the pulse with 1 J of energy. For the case shown in Fig. 8 (B), the energy-normalized peak fluence $F_E(0)$ was found to be 15 kJ/(cm^2 J). Fluctuation level of the normalized peak fluence was found to be 6% based on 100-shot statistics. The peak intensity of the pulse is given by $I_0 = E_L P_E(0) F_E(0) = 17$ EW/cm^2. One can see the significant reduction compared to the one estimated by using the Strehl ratio and a Gaussian spatial profile, 23 EW/cm^2. It demonstrates how significant the effect of non-Gaussian near field profile can be, especially for high power laser system.

As described in Sec. II, a fraction of the laser pulse is first sampled by an uncoated wedge with a 25.4 mm diameter hole. The effect of the hole was studied by replacing the wedge with a wedge without a hole. The presence of the hole was found to decrease the energy-normalized peak fluence by 3% and the fraction of energy in the first minimum by 12%. These effects were taken into account for the evaluations discussed above.

C. Summary for Spatial Domain

As demonstrated here, the BELLA PW laser has delivered high quality spatial modes on target using the ILAO system, where the fraction of energy within the first minimum of the diffraction pattern was found to be 0.75. The Strehl ratio can be a good indicator for performance of a wavefront phase correction system, such as the ILAO system. The effect of the amplitude profile was found to contribute the focus quality

significantly, and therefore, the fraction of energy within the first minimum was introduced to discuss the focus quality in this work. In order to estimate the peak intensity accurately, the energy-normalized fluence was evaluated. For full-energy operation (46 J on target), the peak energy-normalized fluence was found to be 15 kJ/(cm^2 J) with 6% shot-to-shot fluctuation.

Protocols have been established to best handle the thermal aberrations that occur with laser energy changes. Additionally, the excellent quality of the beam allows for measurements such as the channel diagnostics from centroid oscillations of a purposely offset beam [58]. Along with optimization of the spatial quality, efforts have been made to ensure good pointing stability and energy stability as been discussed in Sec. II. Spatial mode optimizations allow for reproducible guiding and more stable electron beams.

IV. Temporal Domain

THE temporal structure of the laser pulse can affect laser-plasma interactions in various ways [1]. Laser pulse self focusing is one of the key phenomena in high power laser-plasma interactions, and depends on the laser power [59]. The laser intensity governs the wake field generation. Laser pulses can evolve significantly during propagation in plasma. A prepulse structure can condition targets before the arrival of the main pulse which may result in performance degradation. The prepulse structure plays a more critical role in laser driven ion accelerations [60] and preliminary experiments are underway to use the BELLA PW laser system to explore this field in the near future [61].

The laser temporal structure can be split into two components, namely the coherent and incoherent portions. The coherent portion, the main structure, can be described as

$$E(t) = \mathscr{F}^{-1}\left\{\sqrt{I(\omega)}\exp[-i\phi(\omega)]\right\}, \qquad (2)$$

where $\mathscr{F}^{-1}$ denotes inverse Fourier transform, I is the laser intensity, ω is the laser angular frequency, and $\phi(\omega)$ is the spectral phase of the pulse. Although the total energy of the laser pulse is ideally contained within 100 fs for typical 30 fs laser pulses, the tail of the pulse can extend to 10 picoseconds or longer due to imperfection in the spectral amplitude and phase from various sources [37], [62]–[65].

The incoherent portion of the pulse typically consists of replicas of the main pulse and contributions from amplified spontaneous emission (ASE) from gain media. For the pre-main structure, it can extend as long as the time duration when the gain media were excited, typically several nanoseconds (can be much longer for post-main structure). The intensity contrast between the main pulse and its prepulses is one of the key parameters in determining the temporal quality of a laser pulse.

In this section, diagnostics, control and performance parameters for the various pulse components are discussed. For the BELLA PW laser system, a photodiode and SEQUOIA, third-order cross-correlator, were used to characterize the incoherent portion of the temporal structure. There have been various techniques developed to characterize femtosecond pulse structure [66]–[69]. In this study, a self-referencing spectral interferometer technique (WIZZLER [70]) and a second-harmonic based frequency resolved optical gating technique (GRENOUILLE [71]) were used to characterize temporal structure. As discussed below, WIZZLER can provide feedback signal to DAZZLER to correct spectral phase of the pulse and GRENOUILLE can provide measurements on spatiotemporal couplings in cost effective way. For all diagnostics mentioned, the laser beam was attenuated through reflections of uncoated wedges or foils, and the whole beam was sent to each diagnostic, rather than sampling a fraction of the beam spatially. Therefore, measurements presented here show spatially-averaged temporal structure at near field.

A. Incoherent Component

In addition to the log-scale nanosecond-long pedestal structure from ASE, pulses can contain multiple pre- and postpulses which typically originate from multiple reflections at plane-parallel optics (pico to nano seconds away from the main pulse) and a pulse train from RA (≥ 1 ns away from the main pulse). Note that through nonlinear processes, a post pulse following the stretched main pulse can result in a prepulse when the main pulse is compressed [72].

For gas-target based LPAs, if such prepulse is intense enough to ionize the gas and arrives early enough for generated electrons to expand, it can lower the plasma density significantly before the arrival of the main pulse [73], [74]. A study indicated that a poor contrast ratio between pre and main pulse resulted in worse electron beam pointing stability and complicated spatial electron beam structure [75]. However, if used correctly, those prepulses can also be utilized to improve LPAs. By carefully arranging prepulses to controllably modify the plasma, they can be used to provide plasma channels to guide intense laser pulses [76], [77] to enhance electron injection to accelerating structure [78], [79]. Although preformed plasma structures can also be created through multiple laser pulses with better flexibility and control [9], [80], [81], the prepulse utilization may have some advantages such as simplified alignment and reduced experimental complexity. For the BELLA PW system, efforts have been made to maximize the contrast to avoid unwanted effects from prepulses.

The control for the incoherent component included configuration of the amplifiers (especially the RA), the XPW, and minimizing the number of plane-parallel optics. The pump lasers' timings were arranged as close to the main laser pulse as reasonably achievable, typically 1 ns before noticeable energy drop in the output energy. The RA's Pockels cell (PC) timing was arranged such that the prepulse contrast was 10 times better than the postpulse. For an ideal condition, the XPW should enhance the contrast $\Upsilon = 0.5\eta_x C_{pol} \sim 8\times10^3$, where $\eta_x \sim 0.17$ is the efficiency of the XPW and $C_{pol} = 10^5$ is the extinction ratio of the polarizers in the XPW.

The nanosecond pulse structure was measured by using a photodiode (DET10A), a 500 MHz bandwidth oscilloscope and calibrated silver-coated pellicle foils (National Photocolor [82]). For the output of the RA, there were pre- and postpulses that originated from the round trip (8.5 ns) as well

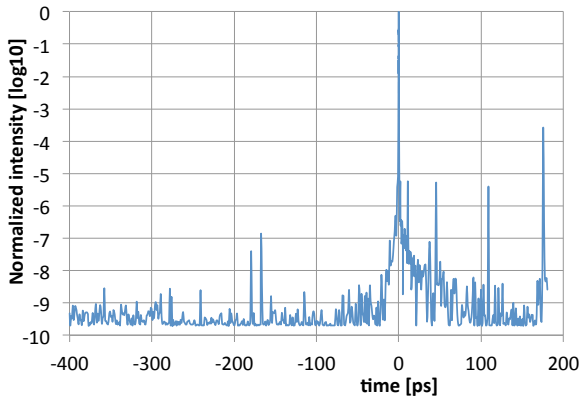

Fig. 10. Sub-nanosecond pulse structure measured by SEQUOIA with 1 ps step and 3-shot averaging at each step. The input energy was about 0.2 mJ.

as a prepulse 3.5 ns away from the main pulse, most likely due to imperfection of the pulse in/out outcoupling inside of the RA. The specifications for the RA indicated that the prepulse contrast was better than 10^3. It was measured to be 2×10^3. After the XPW, it was measured to be 6×10^6, corresponding to 3×10^3 contrast enhancement at the XPW. This somewhat lower contrast enhancement (3×10^3) than analytical estimates (8×10^3) was probably due to the imperfect collimation of the laser pulse at the XPW output polarizer.

The on-target nanosecond structure was measured at the output diagnostic by using an identical setup described above (see Fig. 6 for location). A prepulse 3.5 ns away from the main pulse was observed, but other prepulses observed at the output of the RA (8.5 ns and beyond) were not visible with the same scale probably due to the 1 Hz Pockels cell based pulse cleaner between the booster- and pre-amplifiers (see Fig. 2 for location). The contrast against the 3.5 ns prepulse was measured to be 10^6, an insignificant change from the output of the XPW. With this contrast, the 3.5 ns prepulse was not intense enough to ionize hydrogen or helium gas through optical field ionization, when the focus intensity for the main pulse was estimated to be 17 EW/cm^2.

The sub-nanosecond pulse structure was measured with SEQUOIA at the output diagnostics (see Fig. 6), and shown in Fig. 10. The measurement was done with 1 ps step with 3 shots averaging at each step, and the dynamic range was about 10^9. The input energy was estimated to be about 0.2 mJ. From the measurement, the contrast of the main pulse against ASE pedestal (incoherent portion) was considered to be better than 10^9. The coherent pedestal was visible occupying from -20 to 40 ps range, and is discussed in Sec. IV-B. There were two distinct replicas in front of the main pulse about -175 ps. One of them was considered to be an artifact owing to mixing of the 2nd harmonic of the 175 ps postpulse and the fundamental of the main peak. The other prepulse could be from the nonlinear interference between the main pulse and the postpulse [72]. The source of this postpulse was found to be degraded anti-reflective coating of the Ti:Sapphire crystal in RA. This issue will be addressed in the near future.

B. Coherent Component

The coherent component of the laser pulse temporal profile can be described by Eq. (2), and the spectral phase ϕ can be represented by a Taylor series expansion as,

$$\begin{aligned} \phi(\omega) &= \phi_0 + \phi_1(\omega-\omega_0) + \frac{1}{2!}\phi_2(\omega-\omega_0)^2 \\ &\quad + \frac{1}{3!}\phi_3(\omega-\omega_0)^3 + \frac{1}{4!}\phi_4(\omega-\omega_0)^4 + ..., \quad (3) \\ \phi_n &= \left.\frac{\partial^n \phi}{\partial \omega^n}\right|_{\omega_0}, \end{aligned}$$

where ω_0 is the central angular frequency of the expansion, ϕ_1 is the group velocity of the pulse, ϕ_2 the group velocity dispersion (GVD), and $\phi_n (n \geq 3)$ denotes n-th order dispersion [83], [84]. Described in this section is the optimization process of the spectral phase profile of the pulse.

The control for the coherent component included the angle of incidence to the stretcher and compressor, and diagnostics were the optical spectrometer, WIZZLER and GRENOUILLE. First, the angle of incidence to the stretcher and compressor were adjusted to maximize the energy-normalized peak power. Then the spectral phase profile was further optimized using the DAZZLER.

The angle of incidence to a diffraction grating, α, changes the diffraction angle, β, through the first order grating relation $\sin\alpha + \sin\beta = N\lambda$, where N is the groove density of the grating. The incident angle to the compressor grating pair has an effect on the spectral phase of the pulse coming out from the compressor, ϕ^{cmp}, as [84],

$$\phi^{cmp}(\omega, \beta) = \frac{2\omega L_g \cos\beta}{c}, \quad (4)$$

where L_g is the distance between the gratings and c is the speed of light in vacuum. Through Taylor expansion, one can obtain the dispersion of an arbitrary order $\phi_n^{cmp} = \partial^n \phi^{cmp}/\partial\omega^n|_{\omega 0}$ for the compressor. By varying L_g, one can compensate second order dispersion or ϕ_2. By altering the incident angles to the stretcher and the compressor, one can compensate third (ϕ_3) and fourth (ϕ_4) order dispersion, while also balancing ϕ_2 via appropriate changes for L_g.

The grating incident angle tuning for the second stretcher and compressor was performed while measuring the pulse shape at the output diagnostic. It was found that the highest energy-normalized peak power was obtained when the tails of temporal structure were approximately symmetric. It did not fully eliminate the third and forth order dispersion, but balanced all higher order dispersion to achieve the highest peak power.

Shown in Fig. 11 case (1) is the on-target pulse based on the spectral amplitude measured by the optical spectrometer and the spectral phase measured by the WIZZLER after grating angle tuning. Although the WIZZLER also measured the spectral amplitude, it was measured after many transport optics that modified the spectral amplitude. Based on measurements by the optical spectrometer, and accounting for the sensor response, the on-target spectrum was retrieved. Note that the spectral amplitude for the power below 10^{-3} were modeled with the Gaussian shape pulse detailed in the next paragraph.

This article has been accepted for publication in a future issue of this journal, but has not been fully edited. Content may change prior to final publication. Citation information: DOI 10.1109/JQE.2017.2708601, IEEE Journal of Quantum Electronics

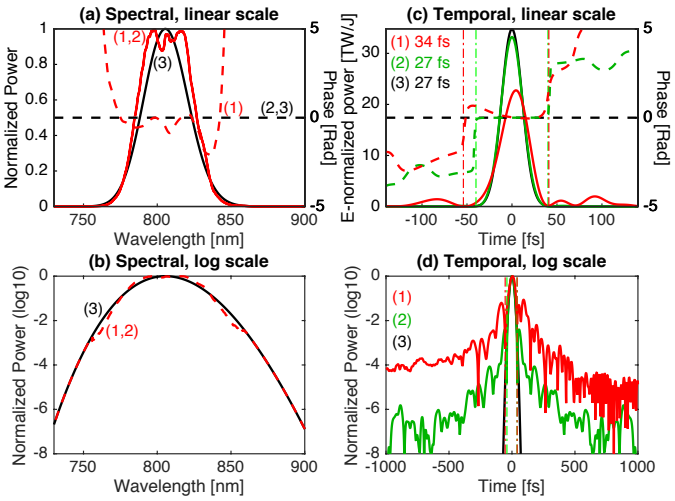

Fig. 11. Three examples of the coherent component, (1, red) measured spectrum amplitude profile $I(\omega)$ (42 nm FWHM) with measured spectral phase by the WIZZLER, (2, green) measured spectral amplitude with a flat spectral phase, and (3, black) a Gaussian spectral amplitude for 35 nm FWHM width with a flat spectral phase. Shown in (a) and (b) are the pulse in spectral domain with linear and log scales, respectively while (c) and (d) show in temporal domain with linear and log scales, respectively. For both linear scale plots, the power is shown by the solid curve with axis on the left side and the phase is shown by the dashed curve with axis on the right side. Temporal pulse width indicated in (c) for each case are in FWHM. Vertical lines in (c) and (d) indicate the location of the first minimum. The spectral phase quality factor for (1) was measured to be 0.68 and a fraction of energy within the first minimum was 0.85 and 0.99 for (1) and (2), respectively.

The spectral phase shift from transmissive optics, such as a vacuum window and a collimation lens, was taken into account, and the shift from reflective optics was neglected.

The vertical axis for Fig. 11 (c) is the energy-normalized power $P_E(t)$ described in Sec. II, and the peak of which, $P_E(0)$, was found to be 23 TW/J. The pulse length in FWHM, τ_{fwhm}, was 34 fs. The pulse peak power is usually estimated simply by $P(0) = E_L/\tau_{fwhm} = 29$ TW for $E_L = 1$ J pulse, overestimating the peak power by more than 20%. This clearly demonstrates that one can not estimate the peak power in this way when a pulse contains significant energy in the tail structure as shown in Fig. 11 (c) case (1).

One can see that the spectral phase was somewhat flat from 770 to 840 nm, but with significant modulation. The spectral phase can be fit with 50th order polynomial, and dispersion up to 4th order were found to be $\phi_2 = -2.2 \times 10^3$ fs^2, $\phi_3 = -1.9 \times 10^6$ fs^3, and $\phi_4 = 1.5 \times 10^8$ fs^4, respectively. As discussed, there were significant amounts of high order dispersion, and they balanced each other to achieve the highest peak power. For such complicated spectral phase structure and the high order polynomial fitting, a discussion on the individual order coefficients is not useful. In order to quantify the quality of spectral phase, a spectral phase quality factor Q_ϕ is defined as,

$$Q_\phi = \frac{P_E(0)|_{\phi=\phi_m}}{P_E(0)|_{\phi=0}}, \tag{5}$$

where ϕ_m is the measured spectral phase. This is identical to the phase error square ϕ^2_{err} defined in Ref. [85], and is conceptually similar to Strehl ratio for spatial domain, for it addresses the quality of spectral phase profile but not of spectral amplitude profile. Shown in Fig. 11 case (2) is a simulated pulse with a measured spectral amplitude $I(\omega)$ with a flat spectral phase $\phi = 0$. The ratio of the energy-normalized peak power between case (1) and (2) gives the spectral quality factor Q_ϕ, and it was found to be 0.68.

In order to study the effects from the spectral amplitude profile, a Gaussian spectral amplitude with a flat spectral phase [$\phi(\omega) = 0$] is calculated and shown in Fig. 11 case (3). The spectral width for case (3) was chosen to be 35 nm FWHM to have the same pulse length in FWHM as case (2). It can be seen that for case (3), the pulse in temporal domain can be contained well within 100 fs even in log scale plot. From Fig. 11 (d), one can see that both spectral amplitude $I(\omega)$ and spectral phase $\phi(\omega)$ can contribute to the construction of the coherent pedestal. Although a significant coherent pedestal was seen in case (2), the peak power was almost the same between cases (1) and (2), indicating shown modulation ($\sim$15%) in the spectral amplitude does not affect the peak power significantly. The modulation in the spectral phase ($\sim$2 rad) significantly reduces the peak power, and increases the coherent pedestal further.

In a similar way to the spatial domain, the fraction of energy within the first minimum can be used to discuss the effect of non-Gaussian spectral amplitude profiles. For Fig. 11, the locations of the first minimum for case (1) and (2) are indicated by the vertical dashed line in (c) and (d), and a fraction of energy within the first minimum for case (1) was 0.85 and (2) was 0.99, respectively. Since case (2) assumes an ideal spectral phase $\phi = 0$, it shows only the effect of spectral amplitude profile, and it was only 1% of energy for this profile.

Although the spectral amplitude was controlled through a DAZZLER as discussed in Sec. II, it was not optimized against the coherent pedestal, but maintained overall bandwidth against gain narrowing. The spectral amplitude defined the pulse shape for chirped (stretched) pulse set by the second stretcher. To ensure that the pulse intensity was below the damage threshold during amplification, this semi-top-hat spectral amplitude, with more than 40 nm FWHM, was maintained. The effects of the picosecond pedestal for femtosecond laser pulse propagation in gas was studied by Giulietti et al. [86], and was found to be not detrimental. For future ion acceleration experiments, the DAZZLER can shape the spectral amplitude closer to a Gaussian amplitude profile if deemed necessary and effective.

In addition to the stretcher/compressor grating angle tuning, the DAZZLER was used to compensate higher order dispersion. The phase measured by the WIZZLER could be directly fed into the DAZZLER for closed loop operation. Here, the feedback operation was done manually to accommodate effects from shot-to-shot fluctuation largely due to pointing fluctuations. First, $\sim$100 shots were taken with the WIZZLER and statistical analysis was performed to remove outlying pulses. Second, after some manipulation (described in next paragraph), the averaged spectral phase was fed into the DAZZLER. This process was repeated till the resultant pulse properties converged. The result of the spectral phase

This article has been accepted for publication in a future issue of this journal, but has not been fully edited. Content may change prior to final publication. Citation information: DOI 10.1109/JQE.2017.2708601, IEEE Journal of Quantum Electronics

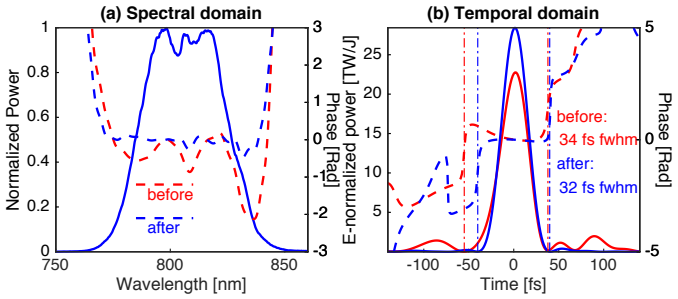

Fig. 12. The laser pulse for before (red) and after (blue) the high order dispersion optimization through the WIZZLER-DAZZLER feedback in (a) spectral domain and (b) temporal domain. The solid curves show the power with the axis on the left side, and the dashed curves show the phase with axis on the right side. The power spectrum were identical for both cases. See Fig. 11 case (3) for details on "before" case. For"after" case, the pulse length was found to be 32 fs in FWHM, the peak power was 28 TW/J, and the spectral phase quality factor was 0.86. Vertical lines in (b) indicate the location of the first minimum. A fraction of energy within the first minimum was 0.85 and 0.97 for "before" and "after", respectively.

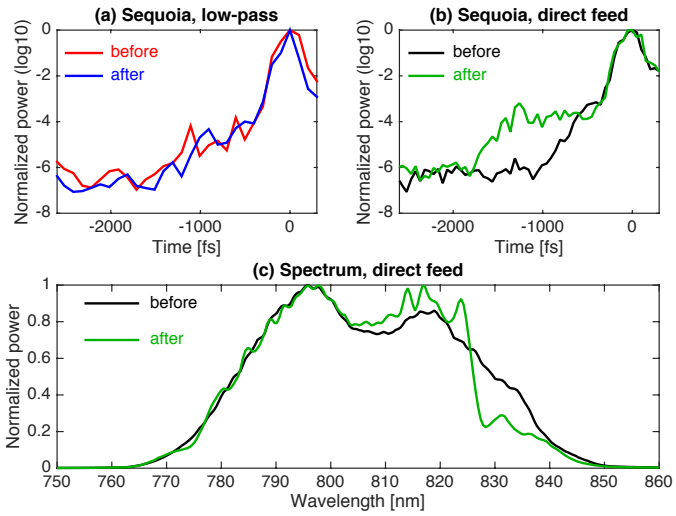

Fig. 13. Picosecond contrast measured by SEQUOIA for (a): low-pass (30th-polynomial-feed) case and (b): direct feed case. The measured optical spectra for before and after the direct feed are shown in (c). The optical spectrum for the 30th-poly-feed case is shown in Fig. 12 (a).

optimization with the WIZZLER-DAZZLER feedback loop is shown in Fig. 12, where the red and blue curves show before [also shown in Fig. 11 case (1)] and after the DAZZLER optimization, respectively. The energy-normalized peak power was improved from 23 to 28 TW/J, the spectral phase quality factor from 0.68 to 0.86, and a fraction of energy within the first minimum from 0.85 to 0.97. The standard deviation of the energy-normalized peak power was measured to be 1%.

The spectral phase quality factor of 0.86 indicates that the spectral phase was not perfectly flat. One can see from Fig. 12 (a) that the spectral phase contains the modulation from remaining higher order dispersion that was purposely not compensated. It was found that when the measured phase was directly fed to the DAZZLER, the resulting spectral amplitude could be modulated. We empirically found that it could be avoided by applying a low-pass filter on the measured spectral phase. The measured and averaged spectral phase was fit by a polynomial, and up to certain orders were included in the phase that was fed to the DAZZLER. For the case shown in Fig. 12, the measured phase was well fit with a 50th order polynomial, and the cut-off order of 30th was found to be a good compromise to achieve the best spectral phase, while not modulating the spectral amplitude. Hence, the measured spectral phase contained the modulation from remaining higher order dispersion.

Figure 13 shows the picosecond time scale pulse structure measured by SEQUOIA for direct feed and 30th order polynomial feed (low-pass) cases. When the low-pass manupilation was applied to the spectral phase, there was no significant difference in picosecond pulse contrast between before and after the DAZZLER optimization as can be seen from Fig. 13 (a). For the case of the direct feed, the modulation on the measured optical spectrum was obvious as shown in Fig. 13 (c), and it resulted in somewhat degraded picosecond contrast of the pulse that is shown in Fig. 13 (b). Note that the spectral amplitude difference between Fig. 12 (a) and Fig. 13 (c) for the "before" case was simply because the measurements were taken on different days, and was not critical for the study of the effect. Though the effects of the picosecond pedestal for femtosecond laser pulse propagation in gas was found to be not detrimental [86], it was optimized in our configuration. The coherent pedestal was found to have the contrast of 10^4 at -0.5 ps, 10^7 at -1.5 ps as shown in Fig. 13 (a), and 10^9 at -20 ps as shown in Fig. 10.

Femtosecond pulse structure was also measured by the GRENOUILLE to confirm the spectral phase optimization. The comparison is shown in Fig. 14 (a) in the spectral domain and (b) in the time domain. The spectral phases measured by the WIZZLER and GRENOUILLE were both averages of about 20 shots. The spectral phase measured by the WIZZLER contains finer structure than that of the GRENOUILLE owing to enhanced spectral resolution, giving an advantage to WIZZLER in measurement accuracy. The comparison in the time domain shows excellent agreement between both diagnostics, with only 3% difference in the energy-normalized peak power.

The spectral phase tuning procedure described above was usually performed with the beam energy significantly below full power (<2 J on target) to avoid any possible risks of damaging optics. Moreover, for pulses above 5 J on-target energy, significant shot-to-shot fluctuation in the spectral amplitude was observed probably due to high accumulated B-integral, namely spectral phase modulation (SPM) [63]. In order to avoid SPM, a gold-coated pellicle foil (average 2.5% transmission over 750 - 850 nm) was inserted before the vacuum window for operations with on-target energy above 5 J (see Fig. 6 for location). Although the foil suppressed shot-to-shot fluctuation in spectral amplitude profile, it has modulated the spectral amplitude because transmission was not spectrally flat. Therefore, the spectral phase tuning was performed with laser energy below 2 J.

With 46 J on target, the spectral phase quality factor was found to degrade to $Q_\phi = 0.76$, the energy normalized peak power was 25 TW/J, and shot-to-shot fluctuation in the energy-normalized peak power was increased from 1%

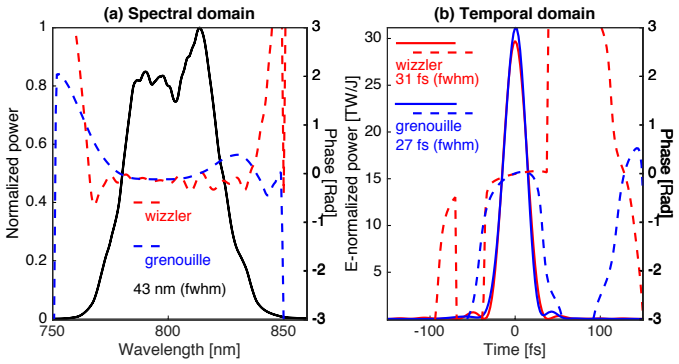

Fig. 14. Femtosecond pulse structure measured by the WIZZLER (red) and the GRENOUILLE (blue) in spectral domain (a) and in temporal domain (b). The solid lines show power on the left side axis and the dashed lines show the phase on the right side axis. The spectral phase quality factor from the WIZZLER was 0.84 and the GRENOUILLE 0.88.

to 5%. One of the possible explanations is SPM due to the high accumulated B-integral. The B-integral at the output diagnostic area was estimated to be $B(46\text{ J}) \sim 4.4$ with the foil before the vacuum window, while $B(2\text{ J}) \sim 3.3$ without the foil. In order to improve, removal of a Faraday rotation isolator between Amp1 and Amp2 (see Fig. 2 for location) and minimization of refractive optics in the system are currently under consideration, which are estimated to reduce 2.3 of the accumulated B-integral at the output diagnostic area.

The source of the observed high order dispersion in the pulse is currently under investigation. There are several possible sources for this high order spectral phase [37], [62]–[65], such as imperfection of the coatings at the spectral edges and contaminated grating surfaces. Since it was observed from low power operation in stable and consistent manner, B-integral was not considered to be a source. It is worth to point out that the BELLA PW system employed one DM to optimize the wavefront at the target, not at the compressor input. A distorted wavefront at the compressor input may contribute to observed high order dispersion. Another DM to optimize wavefront at the input of the compressor may improve the quality of the spectral phase.

As a summary, the optimization process of the spectral phase profile of the pulse was described in this section. The angle of incidence to the stretcher and compressor provided coarse tuning of the spectral phase, and the DAZZLER-WIZZLER feedback process provided fine tuning. Note that the Dazzler had a limitation in the amounts of dispersion that it could compensate. The coarse tuning through the angle of incidence was necessary. The energy-normalized peak power for full power (46 J on target) was 25 TW/J, which gave a peak power of 1.2 PW.

C. Modeling of the Coherent Component

The optimization of the laser temporal profile in terms of obtaining the highest peak power was discussed in Sec. IV-B. The highest laser peak power may not always be the optimum for LPA performance. Depending on applications, LPAs can be tuned to maximize electron beam properties such as charge, energy spread, peak energy. Their performance can be tuned through parameters related to targets such as plasma density, and/or through laser related parameters such as the peak power or pulse length. For example, asymmetric laser pulses yielded the most electron beam charge when somewhat stretched [87]. In staged acceleration scheme [3], [88], one might utilize a longer pulse for post acceleration stages to resonantly excite wakefield for low density plasma and to avoid self-trapping from the highly nonlinear regime.

The compressor grating separation, L_g, is often varied during the LPA optimization processes. A stretched pulse has been usually modeled with a Gaussian shape pulse with deduced GVD from the compressor ϕ_2^{cmp}. If a pulse contains some high order dispersion as shown in the previous section, the temporal amplitude profile may be significantly different from a Gaussian shape, especially when stretched by varying L_g. Accurate knowledge of the temporal amplitude profile and the peak power can be critical to understand and/or model laser plasma interactions [87], [89]. Discussed in this section is a method to model the laser pulse for arbitrary L_g [90].

As shown in Sec. IV-B, WIZZLER and GRENOUILLE can measure femtosecond pulse structure with excellent agreement. While WIZZLER has an advantage in the spectral resolution as well as being capable of single shot measurement without head-tail ambiguity, GRENOUILLE can measure stretched/not optimized pulses consistently for which WIZZLER may not be able to measure accurately. In order to improve accuracy and to overcome the head-tail ambiguity, GRENOUILLE images were taken for multiple L_g. Based on the ϕ_2 change of the compressor with varying L_g, the head-tail ambiguity can be overcome. With the complete model of the optical compressor, one can obtain the dispersion from the compressor $\phi^{cmp}(L_g)$ analytically as shown in Eq. (4). While varying L_g, the dispersion at the diagnostics $\phi^{diag}(L_g)$ would change but not the dispersion for the input pulse to the compressor ϕ^{in},

$$\phi^{in} + \phi^{cmp}(L_g) = \phi^{diag}(L_g). \tag{6}$$

Therefore, by fitting for ϕ^{in} with Grenouille images recorded for multiple L_g, the fitting accuracy can be improved.

Shown in Fig. 15 (a) is an example of GRENOUILLE measurements for multiple L_g. These images were taken for seven locations as indicated by $L_{g'} = L_g - L_{opt}$, where L_{opt} is the optimized grating distance for the highest energy-normalized peak power. At each location 10 images were taken and binned in 3-by-3 pixels to gain dynamic range. Note that the dynamic range of the original single-shot image was 8-bit. One can see that the compressed pulse looks clean in linear scale, while the log scale image reveals fine temporal structure. The input spectral phase ϕ^{in} was fit into a 12th order polynomial by comparing experimental results and simulated GRENOUILLE images, based on ϕ^{in} and spectral amplitude $I(\omega)$ independently measured by the optical spectrometer. The fit results from simulated GRENOUILLE images are shown in Fig. 15 (b). The fit results show agreement with the measured images in linear and log scale. Note that the fit result image assumed spectral and temporal resolution down to one pixel while measured images did not have that resolution.

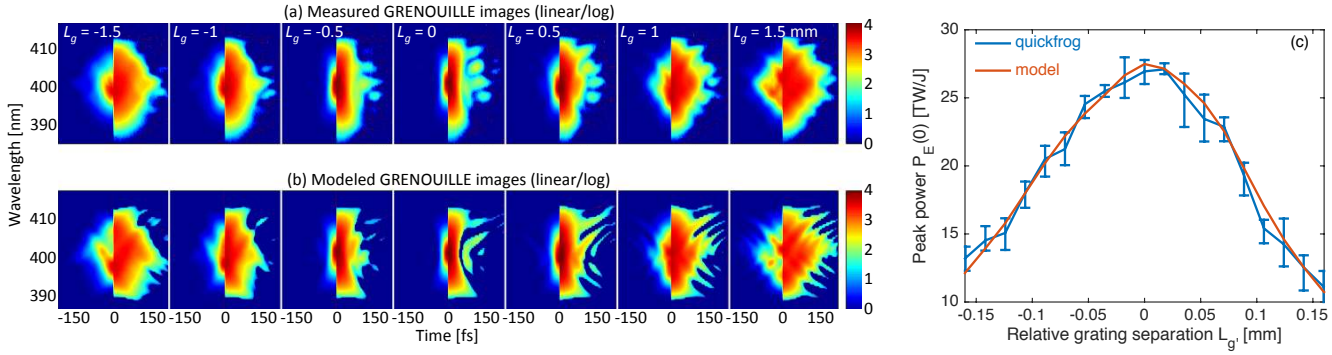

Fig. 15. (a) Measured GRENOUILLE images for multiple $L_{g'} = L_g - L_{opt}$, where L_{opt} is the optimized grating distance. The left side of each image is shown in linear scale and the right side in log scale. The linear scale images were normalized into the peak of the log scale image. For each L_g, 10 shots were acquired, and binned by 3x3 pixels to gain dynamic range. (b) Fit GRENOUILLE images based on the 12th order polynomial ϕ^{in} in log and linear scales. (c) The peak power $P_E(0)$ comparison between Quickfrog analysis and the modeled laser pulse. The errorbar for Quickfrog analysis shows the minimum and maximum of 10 shots acquired for each $L_{g'}$.

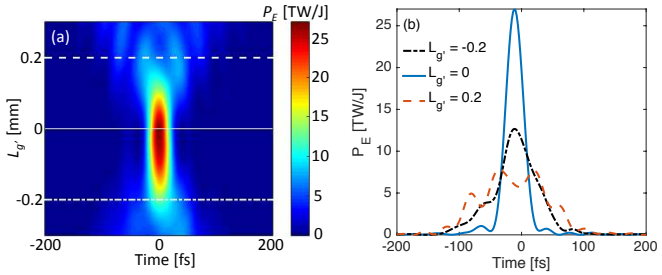

Fig. 16. Modeled temporal pulse profile as a function of $L_{g'}$. (a) Waterfall plot of the pulse temporal profile with color scale showing the power. (b) The modeled temporal profiles for $L_{g'} = -0.2, 0$, and 0.2.

With obtained ϕ^{in}, $I(\omega)$ and ϕ^{cmp}, a pulse shape for arbitrary L_g can be simulated. Shown in Fig. 15 (c) is a comparison between the modeled laser peak power and single-shot analysis done by Quickfrog (Femtosoft) as a function of $L_{g'}$, and their agreement is excellent. The errorbar for Quickfrog analysis shows the minimum and maximum of 10 shots acquired for each $L_{g'}$. With the model, one can simulate pulses for longer $L_{g'}$ where the pulse is difficult to measure.

Figure 16 (a) and (b) show the calculated pulse shape as a function of $L_{g'}$. One can see that when the pulse is stretched with positive $L_{g'}$, it exhibits finer structure that may not be ideal for some applications. Although the modeled pulse shape for the outside of measurable L_g should be validated with other methods, it is far more accurate than the simple Gaussian shape model with only ϕ_2, and precise knowledge of the pulse shape is important to understand complicated laser-plasma interactions.

D. Summary for Temporal Domain

The BELLA PW laser has delivered high quality temporal modes on target with the temporal contrast against ASE higher than 10^9 and the spectral phase quality factor up to 0.86. For full power operation, the energy-normalized peak power was 25 TW/J, or 1.2 PW on target for 46 J beam. The fluctuation of the peak power from the fluctuation of the temporal pulse profile (fluctuation of the laser energy excluded) was found to be 5%. An optimization protocol was established to provide high quality mode in all ns, ps and fs structures. The spectral phase of the pulse exhibited significant high order dispersion. A method to provide an accurate pulse shape for an arbitrary compressor grating distance was presented as well.

V. Spatiotemporal Domain

SPATIAL and temporal properties of ultrashort laser pulses are commonly discussed separately as in previous sections. Since CPA laser systems provide high power laser pulses through the manipulation of spatiotemporal properties, it is inevitable to have some spatiotemporal distortions. Therefore, the separated description of the spatial and temporal properties of the pulse may be valid only when the spatiotemporal distortion is negligibly small for a given application.

One can utilize the spatiotemporal distortions, or spatiotemporal couplings (STCs) when controlled, for some applications. A pulse front tilt can be used to steer electron beams from an LPA [33], to enhance betatron x-ray from an LPA [34], and to pump x-ray lasers efficiently [91]. Wavefront rotation can be used to extract a single attosecond pulse [92]. Simultaneous spatial and temporal focusing [93], [94] is a technique to compress a pulse in time while focusing spatially. It delivers high intensity pulses more localized than conventional ways, and can be useful for applications such as micro machining [95], [96].

Although it is not trivial to characterize STCs of a pulse, there are several techniques available [97]–[104]. Full characterization of STCs for high power lasers requires special care [32]. For a Gaussian beam, all the first-order STCs can be described if beam size w, spectral profile and phase [$I(\omega)$ and $\phi(\omega)$)], angular dispersion, and spatial chirp are known [105]. Discussed in this section are the control and relatively cost-effective way to diagnose the linear angular dispersion and linear spatial chirp (first-order), followed by a model of the first order STCs to simulate evolution of the pulse in the vicinity of focus [106].

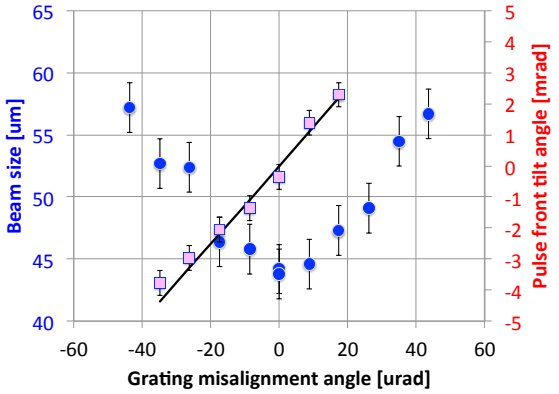

Fig. 17. Far-field spatial chirp measurements with the mode imager (blue circles with left side axis) and near-field pulse front tilt measurement with the GRENOUILLE (red squares with the right side axis) as a function of the misalignment angle of the grating pair δ_g. The beam size is in standard deviation. Pulse front tilt angle was measured at the output diagnostic, where angular dispersion at the diagnostic was $\psi_d = \psi_g/M_d$ and $M_d = 0.015$ is the magnification factor for the diagnostic telescope. Error bars for the beam size is rms of the beam size, and for the pulse front tilt angle is described in the manuscript.

A. Measurements

For a common double-pass optical compressor, a non-parallel grating pair introduces angular dispersion. Angular dispersion, ψ, for a small misalignment angle of the grating pair, δ_g, is described as [33], [92],

$$\psi_g = \frac{d\theta}{d\lambda} = \frac{2N\tan\beta}{\cos\alpha}\delta_g, \tag{7}$$

where ψ_g is angular dispersion at the grating compressor output and θ is the laser propagation angle. For the BELLA PW system, ψ_g [rad/mm] $\sim$ $2.3\delta_g$ [mrad] and could be adjusted with 0.02 rad/mm resolution at the compressor. This corresponds to a grating rotation resolution of 8.7 μrad.

When a laser pulse containing some angular dispersion (at near field) is focused (far field), displacement of the beam at focus exhibits wavelength dependence, $x(\lambda) = f\tan[\theta(\lambda)]$ yielding an elliptic focus, namely spatial chirp. Here, "near field" is defined as the beam at the OAP, and for the BELLA PW system $\psi_{OAP} = \psi_g$. It is common that near-field angular dispersion, ψ_g (or grating parallelism), is tuned by measuring focus intensity profile.

Shown in Fig. 17 by blue circles is the measured horizontal beam size in standard deviation σ_x as a function of δ_g at the output diagnostic mode imager. At each δ_g, the focus location was found by varying z location of the mode imager, and 100 shots were taken at focus. The error bar was from the rms of the beam size. One can see that there is a specific grating angle that provides the smallest beam size (defined as $\delta_g = 0$), and therefore the least ψ_g. The angular dispersion could be minimized within a half δ_g step corresponding to ± 0.01 rad/mm, which was determined by the rotation stage resolution.

When a pulse contains angular dispersion, it exhibits pulse front tilt [107],

$$\tan\gamma_{AD} = \lambda\psi, \tag{8}$$

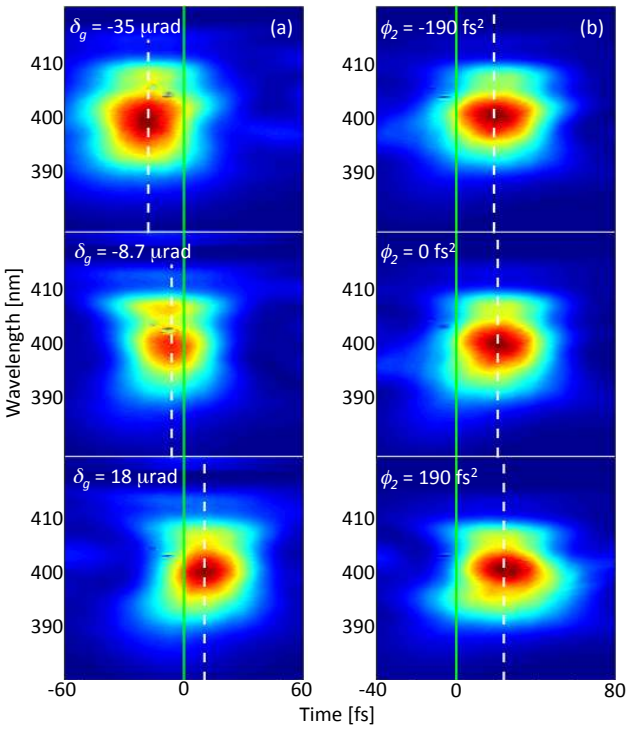

Fig. 18. GRENOUILLE images for pulse front tilt measurement. (a) Grating angle was varied to introduce angular dispersion ψ_g, resulted in different time offset as discussed in the manuscript. Deduced pulse front tilt angle γ was shown in Fig. 17 by the squares. (b) Varied ϕ_2 via grating distance resulted in different time offset ($\psi_g = 0.084$ rad/mm was applied through grating angle misalignment $\delta_g = 37$ μrad). It shows spatial and temporal chirp induced pulse front tilt. Spatial chirp in terms of frequency gradient at the diagnostic was deduced to be $\xi_d = 6 \pm 2 \times 10^{-3}$ (rad/fs)/mm.

where γ_{AD} is pulse front tilt angle from angular dispersion. It was shown that a GRENOUILLE can measure pulse front tilt, where the pulse front tilt results in the acquired image with an offset in time, τ_{os} [108]. This was studied by measuring τ_{os} as a function of δ_g. For this specific GRENOUILLE unit, the relation τ_{os} [fs] $= 4.5\gamma$ [mrad] was obtained from a factory calibration. Note that the product of spatial chirp and temporal chirp also provides pulse front tilt γ_{SC} as described in the following paragraphs, and could contribute to total pulse front tilt angle $\gamma = \gamma_{AD} + \gamma_{SC}$. Therefore, at each angle δ_g, the compressor grating distance L_g was varied to find the position for the least temporal chirp to ensure $\gamma_{SC} = 0$.

The measurement result of pulse front tilt angle by the GRENOUILLE is shown in Fig. 17 (squares, right side axis) together with the expected pulse front angle from Eqs. (7) and (8) (solid line) and were in excellent agreement. Some of the acquired GRENOUILLE images are shown in Fig. 18 (a), where the shift of the offset τ_{os} is visible. Note that the laser pulse went through a telescope with a magnification factor $M_d = 0.015$, which made angular dispersion at the diagnostic $\psi_d = \psi_g/M_d$. The error bar originates from how accurately the center of the GRENOUILLE image could be determined, and was ± 2 pixels ($\gamma = \pm 0.4$ mrad) for the measurements presented here. Although the manufacturer claims sub-pixel resolution of $\gamma = \pm 15$ μrad, which could be true for ideal Gaussian beams, this resolution was not used for the error

bars here.

Two methods to measure the near field angular dispersion are shown in Fig. 17. Focus ellipticity measurement has an advantage in determining 0 dispersion, while GRENOUILLE has to be calibrated by a source with know angular dispersion to determine 0 location. A pulse front tilt measurement with GRENOUILLE has an advantage in measuring angular dispersion directly, while focus ellipticity does not. One can deduce angular dispersion from ellipticity for an ideal Gaussian beam [109] but it is not usually the case. Therefore, it was essential to employ both methods here, determining the 0 dispersion based on the focus measurement and determining the angular dispersion from GRENOUILLE.

There are other techniques to measure angular dispersion such as a spectrally resolved inverted field interferometer [33], [110], which has a typical measurement error of about ± 0.1 rad/mm. The measurement error of the GRENOUILLE presented here was deduced to be ± 0.5 rad/mm, which was 5 times higher. This interferometric technique may have an advantage in resolution and can determine 0 dispersion by itself. It is worth mentioning that the required input beam size for a diagnostic is one of the key parameters for angular dispersion measurements. The measurements presented here required a telescope with a magnification factor $M_d = 0.015$ to match the input beam size for the GRENOUILLE, which was about 2 mm in diameter. This magnified angular dispersion 68 times and the resolution of the GRENOUILLE was sufficient to measure for this work.

For a common double-pass optical compressor, a misaligned retro-reflection mirror introduces spatial chirp [111]. Spatial chirp can also be introduced by propagating a pulse with angular dispersion [109]. Spatial chirp is commonly measured with an imaging optical spectrometer. A shear in the GRENOUILLE image [112] and pulse front tilt caused by spatial and temporal chirp can also be used to measure spatial chirp. Spatial chirp can be defined as the frequency gradient $\xi = d\omega_0/dx$, where ω_0 is the mean angular frequency at position x, and introduces pulse front tilt as [109],

$$\tan \gamma_{SC} = c\phi_2 \xi. \tag{9}$$

Spatial chirp originated pulse front tilt was studied with the GRENOUILLE by varying the compressor grating distance (varying ϕ_2). When angular chirp was minimized ($\delta_g = 0$), no measurable shift in τ_{os} was observed. This indicated that the $\xi_d = \xi_g/M_d$ was below the resolution of the measurement, estimated to be $\pm 2 \times 10^{-3}$ (rad/fs)/mm. Here, ξ_g is near-field frequency gradient and ξ_d is frequency gradient at the diagnostic.

Spatial chirp can be introduced by propagating a beam with angular dispersion. Shown in Fig. 18 (b) is an example where γ_{SC} is large enough to be measured. Angular dispersion $\psi_g = 0.084$ rad/mm was introduced at the compressor via $\delta_g = 37$ μrad, resulted in τ_{os} for the GRENOUILLE image (see middle image). By adding ϕ_2, the offset was slightly varied, as can be seen from the top and the bottom images. Based on this shift in τ_{os}, the frequency gradient was deduced to be $\xi_d = (6 \pm 2) \times 10^{-3}$ (rad/fs)/mm at the GRENOUILLE. The error bar was obtained in the same way as γ_{AD} (2-pixel shift within $\phi_2 = \pm 600$ fs^2) resulting in $\pm 2 \times 10^{-3}$ (rad/fs)/mm. The pulse center of the GRENOUILLE images could be determined well, if the pulse was not stretched too much, $|\phi_2| \leq 600$ fs^2.

It was shown that near-field linear angular dispersion ψ_g and spatial chirp in terms of frequency gradient ξ_g measurements can be obtained through pulse front tilt measurements with GRENOUILLE and focus ellipticity measurements with the mode imager. For the BELLA PW laser, angular dispersion can be adjusted to be $\psi_g = 0 \pm 0.01$ rad/mm using the rotation stage for the compressor grating. Spatial chirp was measured to be below the resolution, $|\xi_g| < 0.03 \times 10^{-3}$ (rad/fs)/mm. When a beam is focused, angular dispersion at near-field becomes spatial chirp at far field and vice versa. It requires a numerical simulation to study STCs at the vicinity of focus, and is described in the following section.

B. Simulation

Spatiotemporal couplings exhibit dynamic behavior near focus, the relevant location for laser-plasma interaction; therefore, simulations of pulses at the vicinity of focus based on the measurement at near-field are important. There are several methods to calculate pulse propagation with spatiotemporal couplings [93], [111], and simplified Fresnel propagation is used in this work.

A Gaussian beam is first defined in x-ω domain at far-field ($z = 0$) as [109],

$$\widetilde{E}(x, \omega, z = 0) = E_0 \exp\left(-\frac{\omega^2 \tau_0^2}{4}\right) \exp\left[-\frac{(x - \zeta_0 \omega)^2}{w_0^2}\right] \exp\left[-i\frac{\phi_2}{2}\omega^2\right] \exp\left(-ik_0 \varphi_0 \omega x\right), \tag{10}$$

where k_0 is the nominal wavenumber and τ_0 defines FL pulse width as $E(t) \propto \exp(-t^2/\tau_0^2)$. The angular dispersion is modeled with $\varphi = d\theta_0/d\omega = -(\lambda^2/2\pi c)\psi$ and the spatial chirp with $\zeta = dx_0/d\omega$, where θ_0 is the propagation angle of this component and x_0 is the beam center position of the ω-component of the beam. The subscript 0 for angular dispersion and spatial chirp indicates that they are defined at far field, i.e., $z = 0$.

By performing a Fourier transform along x, one can obtain the pulse in the k_x-ω domain, where pulse propagation along z can be described by

$$\widehat{E}(k_x, \omega, z = z_1) = \widehat{E}(k_x, \omega, z = 0) \exp\left(jk_z z_1\right), \tag{11}$$

where $k_z = \sqrt{k^2 - k_x^2} \simeq k - k_x^2/2k$ under the paraxial approximation, and the first term k can be neglected since only the diffraction effect is of interest here. Then, an inverse 2D Fourier transform yields the pulse in the x-t domain with arbitrary z, $E(t, x, z = z_1)$.

Since the model above describes the pulse with angular dispersion and spatial chirp defined at the far-field, the relationship between the far-field (simulations) and near-field parameters (measurements) has to be acquired. This can be done by numerically propagating the pulse or by analytically,

$$\varphi_0 \simeq -\frac{f_L}{4}\left(\frac{\lambda_0 \tau_0}{\pi w_0}\right)^2 \xi_g, \tag{12}$$

$$\zeta_0 = -\frac{\lambda^2 f_L}{2\pi c}\psi_g, \tag{13}$$

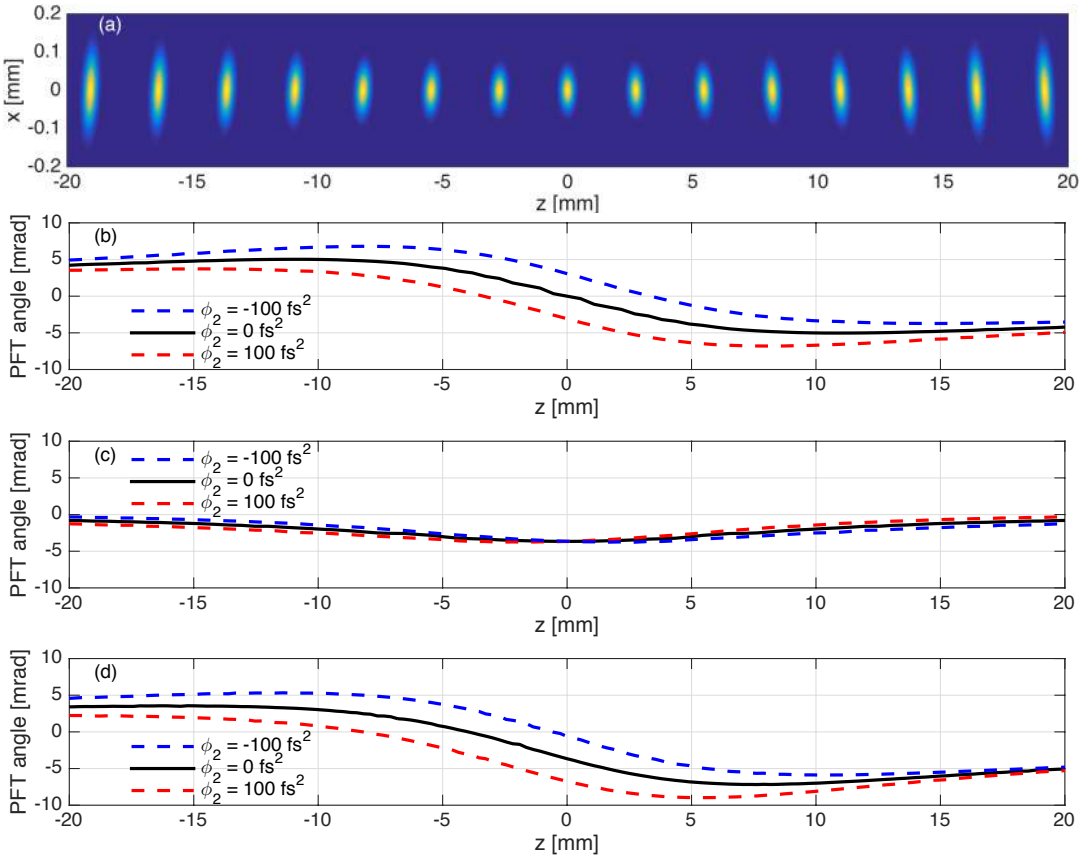

Fig. 19. (a) Visualization of pulse front tilt evolution. The horizontal axis is the propagation distance z and the vertical axis is lateral axis x, where $z = 0$ is focus. For each visualized pulse, width along z was magnified 40 times to visualize pulses. The pulse parameters were $\lambda_0 = 0.81$ μm, $\tau_0 = 25$ fs, $w_0 = 53$ μm, $\phi_2 = 0$, $\xi_g = 0$, and $\psi_g = 0.04$ rad/mm which corresponds to $\delta_g = 18$ μrad. (b-d) Pulse front tilt (PFT) angle γ as a function of propagation distance z for (b) $\psi_g = 0.01$ rad/mm and $\xi_g = 0$, (c) $\psi_g = 0$ and $\xi_g = 0.03 \times 10^{-3}$ (rad/fs)/mm, and (d) $\psi_g = 0.01$ rad/mm and $\xi_n = 0.03 \times 10^{-3}$ (rad/fs)/mm. For all (b-d), $\phi_2 = -100, 0, 100$ fs^2 by dashed blue, solid black, and dashed red lines, respectively.

where f_L is the focal length of a lens. For this study, a Gaussian pulse was modeled with $\tau_0 = 25$ fs, $w_0 = 53$ μm and $\lambda_0 = 0.81$ μm.

Figure 19 (a) illustrates how pulse front tilt dynamically changes at the vicinity of the focus when a pulse has only angular dispersion at the near-field, $\psi_g = 0.04$ rad/mm and $\xi_g = \phi_2 = 0$. Upstream (negative z), the pulse front tilt slowly increases and takes the maximum value at $z = z_R \sim -11$ mm, then decreases to zero at the focus, where the pulse has no angular dispersion but only spatial chirp. Downstream (positive z), pulse front tilt is again present, but with the opposite sign. When there is no near-field spatial chirp nor temporal chirp, $\xi_g = \phi_2 = 0$, the pulse front tilt angle as a function of propagation distance z can be approximated to [113],

$$\gamma(z) \sim \frac{\lambda f_L z}{z_r^2 + z^2} \psi_g, \tag{14}$$

where $\gamma \ll 1$.

The pulse front tilt angle as a function of z is plotted in Fig. 19 (b) for $\psi_g = 0.01$ rad/mm for three ϕ_2 cases, ϕ_2 = -100, 0 and 100 fs^2 shown by dashed blue, solid black, and dashed red lines, respectively. This angular dispersion is equivalent to the error of the measurement discussed in Sec. V-A. Since the pulse has only spatial chirp at focus, pulse front tilt becomes 0 at focus when ϕ_2 is zero. In the vicinity of focus, one can see that ϕ_2 induces some offset to the pulse front angle as shown in Eq. (9). This suggests that off-axis LPA produced electron beams, due to the existence of ψ_g, could be steered by adjusting ϕ_2, namely compressor grating distance.

Shown in Fig. 19 (c) is the pulse front angle when the pulse has only spatial chirp at the near field, $\xi_g = 0.03 \times 10^{-3}$ (rad/fs)/mm and $\psi_g = 0$ for the same three ϕ_2 cases as in Fig. 19 (b). This spatial chirp is equivalent to the error of the measurement discussed in Sec. V-A. In contrast to the case shown in (b), the pulse front angle does not change the sign before and after the focus, and does not change pulse front tilt angle much by varying ϕ_2. When a pulse has spatial chirp at the near field, it exhibits pulse front tilt from angular dispersion γ_{AD} at focus, which does not depend on ϕ_2, as shown in Eq. (8).

In reality, a pulse can have both angular dispersion ψ_g and spatial chirp ξ_g, and Fig. 19 (d) shows the pulse front angle evolution for $\psi_g = 0.01$ rad/mm and $\xi_g = 0.03 \times 10^{-3}$. It illustrates how accurately pulse front tilt can be controlled for the BELLA PW laser based on measurements by GRENOUILLE discussed in Sec. V-A. As can be seen from comparison of (b)-(d), while the pulse front tilt from ψ_g dominates the evolution,

the effect of ξ_g adds small amounts of offset and the effects of ϕ_2 becomes asymmetric. Note that the balance between effects from ψ_g and ξ_g is specific to the system. One can see that the pulse front tilt angle takes its maximum deviation from 0, -7 mrad, at $z = z_R$, indicating that the BELLA PW laser can provide pulses with less than 7 mrad pulse front angle in the vicinity of focus.

Spatial chirp at focus ζ_0 reduces locally available bandwidth, resulting in reduction of the local peak power. For case (d), it was calculated to be 0.32% of peak power reduction. Assuming the same for x and y plane, the power reduction from the residual ζ_0 was estimated to be less than 1%. Spatial chirp increases beam size, resulting in reduction of the fluence. Since the spatial profile measurement discussed in Sec. III includes the effect, correction from ζ_0 for peak fluence is not necessary.

To discuss quality of the pulse in terms of STCs, one could use ψ_g and ξ_g, but resultant pulse front tilt at the vicinity of the focus depends on the focal length f_L and near-field beam size $w_g = w(z = f_L) = f_L\lambda/\pi w_0$. In order to compare quality of the beams with different near-field beam sizes, one may use normalized angular dispersion $\psi_n = \psi_g w_g$ and normalized spatial chirp $\xi_n = \xi_g w_g$. For the BELLA PW system with discussed control and diagnostics, $|\psi_n| < 0.65$ rad and $|\xi_n| < 0.13$ rad/fs can be guaranteed.

One can also evaluate the quality of a laser pulse using the pulse front tilt angle including the effect of focusing optics. Neglecting the effect of ξ_g, the laser pulse exhibits the maximum pulse front tilt at $z = z_R$ as

$$\gamma(z_R) \sim \frac{\pi \tan\beta}{\cos\alpha} \frac{N w_g^2 \delta_g}{f_L}, \tag{15}$$

where $\gamma_{AD} \ll 1$. This implies that the tolerance for δ_g becomes tighter for laser systems with shorter focal length and higher power, which requires larger w_g to mitigate damage threshold of gratings. The grating groove density N also affects the tolerance linearly. As shown in Fig. 19 (b), $\gamma(z_R) \sim 5$ mrad for $\psi_g = 0.01$ rad/mm for BELLA PW laser.

It was shown that near-field linear angular dispersion ψ_g and spatial chirp ξ_g measurements can be obtained through pulse front tilt measurement with GRENOUILLE. Since measurements of temporal profile with GRENOUILLE are essential for any LPA experiments at the BELLA PW facility, the information on the first order STCs can be obtained only with additional analysis. The simulation of the pulse front tilt propagation near focus is presented where the current BELLA PW laser system can guarantee pulse front tilt angle $|\gamma| \leq 7$ mrad near focus, and the reduction of the peak power from STCs was less than 1%. It was also shown that pulse front tilt can be finely tuned through ϕ_2 adjustment.

VI. Summary and Conclusions

DIAGNOSTICS, control and performance parameters for the BELLA PW laser system were discussed. The BELLA PW laser has been built to explore LPA physics. This paper described optimization and control of the high power laser pulses into desired characteristics with necessary diagnostics from a laser user point of view rather than a laser developer point of view.

The main control and diagnostics for the spatial domain are the deformable mirror, wavefront sensor and mode imager, for the temporal domain the angle of incidence to the compressor/stretcher gratings, DAZZLER and WIZZLER, and for spatiotemporal domain the grating angle and GRENOUILLE. The protocols to tune laser parameters for each domain were established and described in the corresponding sections.

The BELLA PW laser provides pulses up to 46 J on target with a percent level energy fluctuation and 1.3 μrad pointing stability. In order to accurately estimate the peak intensity of the laser pulse focus, the energy-normalized peak fluence $F_E(0)$ and energy-normalized peak power $P_E(0)$ were evaluated. For full-energy operation ($E_L = 46$ J), the focus size was measured to be 53 μm, $F_E(0) = 15$ kJ/(cm^2 J) with 6% fluctuation, and $P_E(0) = 25$ TW/J with 5% fluctuation. The peak power was estimated to be $P_0 = E_L P_E(0) = 1.2$ PW and the peak intensity was $I_0 = E_L P_E(0) F_E(0) = 17$ EW/cm^2 with 8% fluctuation.

In order to asses the quality of the mode, the phase quality in Fourier domain (near field wavefront phase for spatial mode and spectral phase for temporal mode) and a fraction of energy within the first minimum of the radial/temporal power distribution (to include both phase and amplitude effects) were evaluated. For the spatial domain, it was found critical to include amplitude distribution effect to discuss the mode quality, due to its large deviation from Gaussian shape. A fraction of energy within the first minimum of the diffraction pattern was 0.75 for the full-energy operation. For the temporal domain, spectral phase quality factor Q_ϕ was found sufficient to discuss temporal mode quality, and $Q_\phi = 0.76$ for the full-energy operation was obtained.

The ns prepulse was measured by a photodiode, and the contrast against 3.5 ns prepulse was measured to be 10^6. The ps contrast was measured with SEQUOIA, and the contrast against ASE pedestal was found to be above 10^9. A method to model the temporal pulse profile for arbitrary compressor-grating separation L_g accurately was discussed.

The first order spatiotemporal couplings were measured by GRENOUILLE, and a simulation of its evolution at the vicinity of focus was presented. The BELLA PW system can provide pulses with less than 7 mrad pulse front tilt angle in the vicinity of focus. The tolerance of pulse front tilts for LPA performance will be studied in the near future.

The work described in this paper has provided performance parameters of the BELLA PW beamline with direct relevance to experiments aimed at exploring a new generation of high energy accelerators. Initial campaigns led to production of up to 4.2 GeV relativistic electron beams from plasma waveguides [26], [27]. These experiments also provided insight in which laser performance aspects are crucial for realizing a multi GeV class laser-plasma accelerator. The performance parameters presented in this paper will provide useful reference to the other high power laser facilities.

ACKNOWLEDGMENT

The authors would like to thank the THALES laser team lead by Francois Lureau for implementation of the BELLA PW laser system, Olivier Chalus for fruitful discussions on the laser system, Jerome Ballesta and Xavier Levecq for implementation of ILAO system, Olivier Albert and Pascal Tournois for support and advices on WIZZLER and DAZZLER, Joe Riley, Steve Fournier, Don Syversrud, Dave Evans, Mark Kirkpatrick, Tyler Sipla, Zachary Eisentraut, Ken Sihler, Nathan Ybarrolaza, Greg Mannino, Ohmar Sowle, Aalhad Deshmukh, Sergio Zimmermann, and the SPE (small projects engineering) group lead by Rob Duarte for technical support, and Sven Steinke, Kelly Swanson, Jeroen van Tilborg, Cameron Geddes, Guillaume Plateau, Remi Lehe, Carlo Benedetti, Stepan Bulanov, Carl Schroeder, and Eric Esarey for their contributions.

REFERENCES

[1] E. Esarey, C. B. Schroeder, and W. P. Leemans, "Physics of laser-driven plasma-based electron accelerators," *Rev. Mod. Phys.*, vol. 81, pp. 1229–1285, Aug 2009. [Online]. Available: https://link.aps.org/doi/10.1103/RevModPhys.81.1229

[2] W. P. Leemans and E. Esarey, "Laser-driven plasma-wave electron accelerators," *Physics today*, vol. 62, p. 44, 2009.

[3] C. B. Schroeder, E. Esarey, and W. P. Leemans, "Beamstrahlung considerations in laser-plasma-accelerator-based linear colliders," *Phys. Rev. ST Accel. Beams*, vol. 15, p. 051301, May 2012. [Online]. Available: http://link.aps.org/doi/10.1103/PhysRevSTAB.15.051301

[4] A. R. Maier, A. Meseck, S. Reiche, C. B. Schroeder, T. Seggebrock, and F. Grüner, "Demonstration scheme for a laser-plasma-driven free-electron laser," *Phys. Rev. X*, vol. 2, p. 031019, Sep 2012. [Online]. Available: http://link.aps.org/doi/10.1103/PhysRevX.2.031019

[5] J. Faure, B. van der Geer, B. Beaurepaire, G. Gallé, A. Vernier, and A. Lifschitz, "Concept of a laser-plasma-based electron source for sub-10-fs electron diffraction," *Phys. Rev. Accel. Beams*, vol. 19, p. 021302, Feb 2016. [Online]. Available: http://link.aps.org/doi/10.1103/PhysRevAccelBeams.19.021302

[6] F. Albert and A. G. R. Thomas, "Applications of laser wakefield accelerator-based light sources," *Plasma Physics and Controlled Fusion*, vol. 58, no. 10, p. 103001, 2016. [Online]. Available: http://stacks.iop.org/0741-3335/58/i=10/a=103001

[7] D. Strickland and G. Mourou, "Compression of amplified chirped optical pulses," *Optics Communications*, vol. 56, no. 3, pp. 219 – 221, 1985. [Online]. Available: http://www.sciencedirect.com/science/article/pii/0030401885901208

[8] S. P. D. Mangles, C. D. Murphy, Z. Najmudin, A. G. R. Thomas, J. L. Collier, A. E. Dangor, E. J. Divall, P. S. Foster, J. G. Gallacher, C. J. Hooker, D. A. Jaroszynski, A. J. Langley, W. B. Mori, P. A. Norreys, F. S. Tsung, R. Viskup, B. R. Walton, and K. Krushelnick, "Monoenergetic beams of relativistic electrons from intense laser-plasma interactions," *Nature*, vol. 431, no. 7008, pp. 535–538, 09 2004. [Online]. Available: http://dx.doi.org/10.1038/nature02939

[9] C. G. R. Geddes, C. Toth, J. van Tilborg, E. Esarey, C. B. Schroeder, D. Bruhwiler, C. Nieter, J. Cary, and W. P. Leemans, "High-quality electron beams from a laser wakefield accelerator using plasma-channel guiding," *Nature*, vol. 431, no. 7008, pp. 538–541, 09 2004. [Online]. Available: http://dx.doi.org/10.1038/nature02900

[10] J. Faure, Y. Glinec, A. Pukhov, S. Kiselev, S. Gordienko, E. Lefebvre, J. P. Rousseau, F. Burgy, and V. Malka, "A laser-plasma accelerator producing monoenergetic electron beams," *Nature*, vol. 431, no. 7008, pp. 541–544, 09 2004. [Online]. Available: http://dx.doi.org/10.1038/nature02963

[11] W. P. Leemans, B. Nagler, A. J. Gonsalves, C. Toth, K. Nakamura, C. G. R. Geddes, E. Esarey, C. B. Schroeder, and S. M. Hooker, "Gev electron beams from a centimetre-scale accelerator," *Nat Phys*, vol. 2, no. 10, pp. 696–699, 10 2006. [Online]. Available: http://dx.doi.org/10.1038/nphys418

[12] N. A. M. Hafz, T. M. Jeong, I. W. Choi, S. K. Lee, K. H. Pae, V. V. Kulagin, J. H. Sung, T. J. Yu, K.-H. Hong, T. Hosokai, J. R. Cary, D.-K. Ko, and J. Lee, "Stable generation of gev-class electron beams from self-guided laser-plasma channels," *Nat Photon*, vol. 2, no. 9, pp. 571–577, 09 2008. [Online]. Available: http://dx.doi.org/10.1038/nphoton.2008.155

[13] T. P. A. Ibbotson, N. Bourgeois, T. P. Rowlands-Rees, L. S. Caballero, S. I. Bajlekov, P. A. Walker, S. Kneip, S. P. D. Mangles, S. R. Nagel, C. A. J. Palmer, N. Delerue, G. Doucas, D. Urner, O. Chekhlov, R. J. Clarke, E. Divall, K. Ertel, P. S. Foster, S. J. Hawkes, C. J. Hooker, B. Parry, P. P. Rajeev, M. J. V. Streeter, and S. M. Hooker, "Laser-wakefield acceleration of electron beams in a low density plasma channel," *Phys. Rev. ST Accel. Beams*, vol. 13, p. 031301, Mar 2010. [Online]. Available: http://link.aps.org/doi/10.1103/PhysRevSTAB.13.031301

[14] C. E. Clayton, J. E. Ralph, F. Albert, R. A. Fonseca, S. H. Glenzer, C. Joshi, W. Lu, K. A. Marsh, S. F. Martins, W. B. Mori, A. Pak, F. S. Tsung, B. B. Pollock, J. S. Ross, L. O. Silva, and D. H. Froula, "Self-guided laser wakefield acceleration beyond 1 gev using ionization-induced injection," *Phys. Rev. Lett.*, vol. 105, p. 105003, Sep 2010. [Online]. Available: https://link.aps.org/doi/10.1103/PhysRevLett.105.105003

[15] X. Wang, R. Zgadzaj, N. Fazel, Z. Li, S. A. Yi, X. Zhang, W. Henderson, Y. Y. Chang, R. Korzekwa, H. E. Tsai, C. H. Pai, H. Quevedo, G. Dyer, E. Gaul, M. Martinez, A. C. Bernstein, T. Borger, M. Spinks, M. Donovan, V. Khudik, G. Shvets, T. Ditmire, and M. C. Downer, "Quasi-monoenergetic laser-plasma acceleration of electrons to 2 gev," *Nature Communications*, vol. 4, pp. 1988 EP –, 06 2013. [Online]. Available: http://dx.doi.org/10.1038/ncomms2988

[16] H. T. Kim, K. H. Pae, H. J. Cha, I. J. Kim, T. J. Yu, J. H. Sung, S. K. Lee, T. M. Jeong, and J. Lee, "Enhancement of electron energy to the multi-gev regime by a dual-stage laser-wakefield accelerator pumped by petawatt laser pulses," *Phys. Rev. Lett.*, vol. 111, p. 165002, Oct 2013. [Online]. Available: http://link.aps.org/doi/10.1103/PhysRevLett.111.165002

[17] W. Leemans, J. Daniels, A. Deshmukh, A. J. Gonsalves, A. Magana, H. S. Mao, D. E. Mittelberger, K. Nakamura, J. R. Riley, D. Syversrud, C. Toth, and N. Ybarrolazza, "Bella laser and operations," in *Proceedings of the 2013 Particle Accelerator Conference*, Pasadena, CA, 2013, p. 1097.

[18] THALES. [Online]. Available: www.thalesgroup.com

[19] C. Danson, D. Hillier, N. Hopps, and D. Neely, "Petawatt class lasers worldwide," *High Power Laser Science and Engineering*, vol. 3, p. e3, 2015.

[20] C. J. Hooker, J. L. Collier, O. Chekhlov, R. J. Clarke, E. J. DivallI, K. Ertel, P. Foster, S. Hancock, S. J. Hawkes, P. Holligan, A. J. Langley, W. J. Lester, D. Neely, B. T. Parry, and B. E. Wyborn, "The astra gemini petawatt ti:sapphire laser," *Review of Lasear Engineering*, vol. 37, p. 443, 2009.

[21] E. W. Gaul, M. Martinez, J. Blakeney, A. Jochmann, M. Ringuette, D. Hammond, T. Borger, R. Escamilla, S. Douglas, W. Henderson, G. Dyer, A. Erlandson, R. Cross, J. Caird, C. Ebbers, and T. Ditmire, "Demonstration of a 1.1 petawatt laser based on a hybrid optical parametric chirped pulse amplification/mixed nd:glass amplifier," *Appl. Opt.*, vol. 49, no. 9, pp. 1676–1681, Mar 2010. [Online]. Available: http://ao.osa.org/abstract.cfm?URI=ao-49-9-1676

[22] H. Kiriyama, M. Mori, A. S. Pirozhkov, K. Ogura, A. Sagisaka, A. Kon, T. Z. Esirkepov, Y. Hayashi, H. Kotaki, M. Kanasaki, H. Sakaki, Y. Fukuda, J. Koga, M. Nishiuchi, M. Kando, S. V. Bulanov, K. Kondo, P. R. Bolton, O. Slezak, D. Vojna, M. Sawicka-Chyla, V. Jambunathan, A. Lucianetti, and T. Mocek, "High-contrast, high-intensity petawatt-class laser and applications," *IEEE Journal of Selected Topics in Quantum Electronics*, vol. 21, no. 1, pp. 232–249, Jan 2015.

[23] T. J. Yu, S. K. Lee, J. H. Sung, J. W. Yoon, T. M. Jeong, and J. Lee, "Generation of high-contrast, 30 fs, 1.5 pw laser pulses from chirped-pulse amplification ti:sapphire laser," *Opt. Express*, vol. 20, no. 10, pp. 10 807–10 815, May 2012. [Online]. Available: http://www.opticsexpress.org/abstract.cfm?URI=oe-20-10-10807

[24] Y. Chu, Z. Gan, X. Liang, L. Yu, X. Lu, C. Wang, X. Wang, L. Xu, H. Lu, D. Yin, Y. Leng, R. Li, and Z. Xu, "High-energy large-aperture ti:sapphire amplifier for 5 pw laser pulses," *Opt. Lett.*, vol. 40, no. 21, pp. 5011–5014, Nov 2015. [Online]. Available: http://ol.osa.org/abstract.cfm?URI=ol-40-21-5011

[25] P. L. Poole, C. Willis, R. L. Daskalova, K. M. George, S. Feister, S. Jiang, J. Snyder, J. Marketon, D. W. Schumacher, K. U. Akli, L. V. Woerkom, R. R. Freeman, and E. A. Chowdhury, "Experimental capabilities of 0.4 pw, 1 shot/min scarlet laser facility for high energy density science," *Appl. Opt.*, vol. 55, no. 17, pp. 4713–4719, Jun 2016. [Online]. Available: http://ao.osa.org/abstract.cfm?URI=ao-55-17-4713

[26] W. P. Leemans, A. J. Gonsalves, H.-S. Mao, K. Nakamura, C. Benedetti, C. B. Schroeder, C. Tóth, J. Daniels, D. E.

Mittelberger, S. S. Bulanov, J.-L. Vay, C. G. R. Geddes, and E. Esarey, "Multi-gev electron beams from capillary-discharge-guided subpetawatt laser pulses in the self-trapping regime," *Phys. Rev. Lett.*, vol. 113, p. 245002, Dec 2014. [Online]. Available: http://link.aps.org/doi/10.1103/PhysRevLett.113.245002

[27] A. J. Gonsalves, K. Nakamura, J. Daniels, H.-S. Mao, C. Benedetti, C. B. Schroeder, C. Tóth, J. van Tilborg, D. E. Mittelberger, S. S. Bulanov, J.-L. Vay, C. G. R. Geddes, E. Esarey, and W. P. Leemans, "Generation and pointing stabilization of multi-gev electron beams from a laser plasma accelerator driven in a pre-formed plasma waveguidea)," *Physics of Plasmas*, vol. 22, no. 5, p. 056703, 2015. [Online]. Available: http://scitation.aip.org/content/aip/journal/pop/22/5/10.1063/1.4919278

[28] A. Butler, D. J. Spence, and S. M. Hooker, "Guiding of high-intensity laser pulses with a hydrogen-filled capillary discharge waveguide," *Phys. Rev. Lett.*, vol. 89, p. 185003, Oct 2002. [Online]. Available: https://link.aps.org/doi/10.1103/PhysRevLett.89.185003

[29] A. J. Gonsalves, T. P. Rowlands-Rees, B. H. P. Broks, J. J. A. M. van der Mullen, and S. M. Hooker, "Transverse interferometry of a hydrogen-filled capillary discharge waveguide," *Phys. Rev. Lett.*, vol. 98, p. 025002, Jan 2007. [Online]. Available: https://link.aps.org/doi/10.1103/PhysRevLett.98.025002

[30] A. Pukhov and J. Meyer-ter Vehn, "Laser wake field acceleration: the highly non-linear broken-wave regime," *Applied Physics B*, vol. 74, no. 4, pp. 355–361, 2002. [Online]. Available: http://dx.doi.org/10.1007/s003400200795

[31] S. Shiraishi, C. Benedetti, A. J. Gonsalves, K. Nakamura, B. H. Shaw, T. Sokollik, J. van Tilborg, C. G. R. Geddes, C. B. Schroeder, C. Tóth, E. Esarey, and W. P. Leemans, "Laser red shifting based characterization of wakefield excitation in a laser-plasma accelerator," *Physics of Plasmas*, vol. 20, no. 6, p. 063103, 2013. [Online]. Available: http://scitation.aip.org/content/aip/journal/pop/20/6/10.1063/1.4810802

[32] G. Pariente, V. Gallet, A. Borot, O. Gobert, and F. Quéré, "Space–time characterization of ultra-intense femtosecond laser beams," *Nat Photon*, vol. 10, no. 8, pp. 547–553, 08 2016. [Online]. Available: http://dx.doi.org/10.1038/nphoton.2016.140

[33] A. Popp, J. Vieira, J. Osterhoff, Z. Major, R. Hörlein, M. Fuchs, R. Weingartner, T. P. Rowlands-Rees, M. Marti, R. A. Fonseca, S. F. Martins, L. O. Silva, S. M. Hooker, F. Krausz, F. Grüner, and S. Karsch, "All-optical steering of laser-wakefield-accelerated electron beams," *Phys. Rev. Lett.*, vol. 105, p. 215001, Nov 2010. [Online]. Available: https://link.aps.org/doi/10.1103/PhysRevLett.105.215001

[34] M. Schnell, A. Sävert, I. Uschmann, M. Reuter, M. Nicolai, T. Kämpfer, B. Landgraf, O. Jäckel, O. Jansen, A. Pukhov, M. C. Kaluza, and C. Spielmann, "Optical control of hard x-ray polarization by electron injection in a laser wakefield accelerator," *Nature Communications*, vol. 4, pp. 2421 EP –, 09 2013. [Online]. Available: http://dx.doi.org/10.1038/ncomms3421

[35] N. Minkovski, G. I. Petrov, S. M. Saltiel, O. Albert, and J. Etchepare, "Nonlinear polarization rotation and orthogonal polarization generation experienced in a single-beam configuration," *J. Opt. Soc. Am. B*, vol. 21, no. 9, pp. 1659–1664, Sep 2004. [Online]. Available: http://josab.osa.org/abstract.cfm?URI=josab-21-9-1659

[36] Coherent. [Online]. Available: www.coherent.com

[37] D. Kaganovich, J. R. Penano, M. H. Helle, D. F. Gordon, B. Hafizi, and A. Ting, "Origin and control of the subpicosecond pedestal in femtosecond laser systems," *Opt. Lett.*, vol. 38, no. 18, pp. 3635–3638, Sep 2013. [Online]. Available: http://ol.osa.org/abstract.cfm?URI=ol-38-18-3635

[38] A. Jullien, L. Canova, O. Albert, D. Boschetto, L. Antonucci, Y.-H. Cha, J. Rousseau, P. Chaudet, G. Chériaux, J. Etchepare, S. Kourtev, N. Minkovski, and S. Saltiel, "Spectral broadening and pulse duration reduction during cross-polarized wave generation: influence of the quadratic spectral phase," *Applied Physics B*, vol. 87, no. 4, pp. 595–601, 2007. [Online]. Available: http://dx.doi.org/10.1007/s00340-007-2685-8

[39] Fastlite. [Online]. Available: www.fastlite.com

[40] A. Jullien, O. Albert, G. Chériaux, J. Etchepare, S. Kourtev, N. Minkovski, and S. M. Saltiel, "A two crystal arrangement to fight efficiency saturation in cross-polarized wave generation," *Opt. Express*, vol. 14, no. 7, pp. 2760–2769, Apr 2006. [Online]. Available: http://www.opticsexpress.org/abstract.cfm?URI=oe-14-7-2760

[41] L. Canova, O. Albert, N. Forget, B. Mercier, S. Kourtev, N. Minkovski, S. Saltiel, and R. Lopez Martens, "Influence of spectral phase on cross-polarized wave generation with short femtosecond pulses," *Applied Physics B*, vol. 93, no. 2-3, pp. 443–453, 2008. [Online]. Available: http://dx.doi.org/10.1007/s00340-008-3185-1

[42] Imagine optic. [Online]. Available: www.imagine-optic.com

[43] Gentec-eo. [Online]. Available: www.gentec-eo.com

[44] K. Nakamura, W. Wan, N. Ybarrolaza, D. Syversrud, J. Wallig, and W. P. Leemans, "Broadband single-shot electron spectrometer for gev-class laser-plasma-based accelerators," *Rev. Sci. Instrum.*, vol. 79, no. 5, p. 053301, 2008. [Online]. Available: http://link.aip.org/link/?RSI/79/053301/1

[45] K. Nakamura, A. J. Gonsalves, C. Lin, A. Smith, D. Rodgers, R. Donahue, W. Byrne, and W. P. Leemans, "Electron beam charge diagnostics for laser plasma accelerators," *Phys. Rev. ST Accel. Beams*, vol. 14, p. 062801, Jun 2011. [Online]. Available: https://link.aps.org/doi/10.1103/PhysRevSTAB.14.062801

[46] K. Nakamura, D. E. Mittelberger, A. J. Gonsalves, J. Daniels, H.-S. Mao, F. Stulle, J. Bergoz, and W. P. Leemans, "Pico-coulomb charge measured at bella to percent-level precision using a turbo-ict," *Plasma Physics and Controlled Fusion*, vol. 58, no. 3, p. 034010, 2016. [Online]. Available: http://stacks.iop.org/0741-3335/58/i=3/a=034010

[47] Hamamatsu photonics. [Online]. Available: www.hamamatsu.com

[48] Swamp optics. [Online]. Available: www.swampoptics.com

[49] Amplitude technologies. [Online] www.amplitude-technologies.com

[50] Thorlabs. [Online]. Available: www.thorlabs.com

[51] N. Nakanii, T. Hosokai, K. Iwasa, N. C. Pathak, S. Masuda, A. G. Zhidkov, H. Nakahara, N. Takeguchi, Y. Mizuta, T. P. Otsuka, K. Sueda, H. Nakamura, and R. Kodama, "Effect of halo on the stability of electron bunches in laser wakefield acceleration," *EPL (Europhysics Letters)*, vol. 113, no. 3, p. 34002, 2016. [Online]. Available: http://stacks.iop.org/0295-5075/113/i=3/a=34002

[52] N. Lefaudeux, X. Levecq, G. Dovillaire, S. Theis, and L. Escolano, "New deformable mirror technology and associated control strategies for ultrahigh intensity laser beam corrections and optimizations," in *Proc. SPIE 8236, Laser Resonators, Microresonators, and Beam Control XIV*, vol. 8236, 2012, pp. 82 360K–6. [Online]. Available: http://dx.doi.org/10.1117/12.907180

[53] H.-S. Mao, K. Nakamura, A. J. Gonsalves, C. Tóth, and W. P. Leemans, "High-quality spatial modes for petawatt-class lasers," *AIP Conference Proceedings*, vol. 1777, no. 1, p. 110003, 2016. [Online]. Available: http://aip.scitation.org/doi/abs/10.1063/1.4965692

[54] S.-W. Bahk, P. Rousseau, T. A. Planchon, V. Chvykov, G. Kalintchenko, A. Maksimchuk, G. A. Mourou, and V. Yanovsky, "Generation and characterization of the highest laser intensities (1022 w/cm2)," *Opt. Lett.*, vol. 29, no. 24, pp. 2837–2839, Dec 2004. [Online]. Available: http://ol.osa.org/abstract.cfm?URI=ol-29-24-2837

[55] T. S. Ross and W. P. Latham, "Appropriate measures and consistent standard for high energy laser beam quality," *Journal of Directed Energy*, vol. 2, p. 22, 2006.

[56] E. Perevezentsev, A. Poteomkin, and E. Khazanov, "Comparison of laser beam quality criteria," in *Laser Beam Control and Applications*, vol. 6101, 2006, pp. 610 119–610 119–11. [Online]. Available: http://dx.doi.org/10.1117/12.644632

[57] V. N. Mahajan, "Strehl ratio for primary aberrations in terms of their aberration variance," *J. Opt. Soc. Am.*, vol. 73, no. 6, pp. 860–861, Jun 1983. [Online]. Available: http://www.osapublishing.org/abstract.cfm?URI=josa-73-6-860

[58] A. J. Gonsalves, K. Nakamura, C. Lin, J. Osterhoff, S. Shiraishi, C. B. Schroeder, C. G. R. Geddes, C. Toth, E. Esarey, and W. P. Leemans, "Plasma channel diagnostic based on laser centroid oscillations," *Phys. Plasmas*, vol. 17, no. 5, p. 056706, 2010. [Online]. Available: http://link.aip.org/link/?PHP/17/056706/1

[59] P. Sprangle, C. M. Tang, and E. Esarey, "Relativistic self-focusing of short-pulse radiation beams in plasmas," *IEEE Transactions on Plasma Science*, vol. 15, no. 2, pp. 145–153, April 1987.

[60] J. Schreiber, P. R. Bolton, and K. Parodi, "Invited review article: "hands-on" laser-driven ion acceleration: A primer for laser-driven source development and potential applications," *Review of Scientific Instruments*, vol. 87, no. 7, 2016. [Online]. Available: http://scitation.aip.org/content/aip/journal/rsi/87/7/10.1063/1.4959198

[61] C. Toth, D. Evans, A. J. Gonsalves, M. Kirkpatrick, A. Magana, G. Mannino, H.-S. Mao, K. Nakamura, J. R. Riley, S. Steinke, T. Sipla, D. Syversrud, N. Ybarrolaza, and W. P. Leemans, "Transition of the bella pw laser system towards a collaborative research facility in laser plasma science," *AIP Conference Proceedings*, vol. 1812, no. 1, p. 110005, 2017. [Online]. Available: http://aip.scitation.org/doi/abs/10.1063/1.4975918

[62] C. Hooker, Y. Tang, O. Chekhlov, J. Collier, E. Divall, K. Ertel, S. Hawkes, B. Parry, and P. P. Rajeev, "Improving

coherent contrast of petawatt laser pulses," *Opt. Express*, vol. 19, no. 3, pp. 2193–2203, Jan 2011. [Online]. Available: http://www.opticsexpress.org/abstract.cfm?URI=oe-19-3-2193

[63] M. D. Perry, T. Ditmire, and B. C. Stuart, "Self-phase modulation in chirped-pulse amplification," *Opt. Lett.*, vol. 19, no. 24, pp. 2149–2151, Dec 1994. [Online]. Available: http://ol.osa.org/abstract.cfm?URI=ol-19-24-2149

[64] C. V. Filip, "Computers at work on ultrafast laser design," *Opt. Photon. News*, vol. 23, no. 5, pp. 24–29, May 2012. [Online]. Available: http://www.osa-opn.org/abstract.cfm?URI=opn-23-5-24

[65] C. Danson, D. Neely, and D. Hillier, "Pulse fidelity in ultra-high-power (petawatt class) laser systems," *High Power Laser Science and Engineering*, vol. 2, p. e34, 2014.

[66] I. A. Walmsley and C. Dorrer, "Characterization of ultrashort electromagnetic pulses," *Adv. Opt. Photon.*, vol. 1, no. 2, pp. 308–437, Apr 2009. [Online]. Available: http://aop.osa.org/abstract.cfm?URI=aop-1-2-308

[67] R. Trebino, K. W. DeLong, D. N. Fittinghoff, J. N. Sweetser, M. A. Krumbügel, B. A. Richman, and D. J. Kane, "Measuring ultrashort laser pulses in the time-frequency domain using frequency-resolved optical gating," *Review of Scientific Instruments*, vol. 68, no. 9, pp. 3277–3295, 1997. [Online]. Available: http://dx.doi.org/10.1063/1.1148286

[68] F. Böhle, M. Kretschmar, A. Jullien, M. Kovacs, M. Miranda, R. Romero, H. Crespo, U. Morgner, P. Simon, R. Lopez-Martens, and T. Nagy, "Compression of cep-stable multi-mj laser pulses down to 4fs in long hollow fibers," *Laser Physics Letters*, vol. 11, no. 9, p. 095401, 2014. [Online]. Available: http://stacks.iop.org/1612-202X/11/i=9/a=095401

[69] D. E. Mittelberger, K. Nakamura, R. Lehe, A. J. Gonsalves, C. Benedetti, H.-S. Mao, J. Daniels, N. Dale, S. V. Venkatakrishnan, K. K. Swanson, E. Esarey, and W. P. Leemans, "Characterization of the spectral phase of an intense laser at focus via ionization blueshift," *J. Opt. Soc. Am. B*, vol. 33, no. 9, pp. 1978–1985, Sep 2016. [Online]. Available: http://josab.osa.org/abstract.cfm?URI=josab-33-9-1978

[70] T. Oksenhendler, S. Coudreau, N. Forget, V. Crozatier, S. Grabielle, R. Herzog, O. Gobert, and D. Kaplan, "Self-referenced spectral interferometry," *Applied Physics B*, vol. 99, no. 1-2, pp. 7–12, 2010. [Online]. Available: http://dx.doi.org/10.1007/s00340-010-3916-y

[71] P. O'Shea, M. Kimmel, X. Gu, and R. Trebino, "Highly simplified device for ultrashort-pulse measurement," *Opt. Lett.*, vol. 26, no. 12, pp. 932–934, Jun 2001. [Online]. Available: http://ol.osa.org/abstract.cfm?URI=ol-26-12-932

[72] N. Didenko, A. Konyashchenko, A. Lutsenko, and S. Tenyakov, "Contrast degradation in a chirped-pulse amplifier due to generation of prepulses by postpulses," *Opt. Express*, vol. 16, no. 5, pp. 3178–3190, Mar 2008. [Online]. Available: http://www.opticsexpress.org/abstract.cfm?URI=oe-16-5-3178

[73] S. Masuda and E. Miura, "Effect of femtosecond prepulse with threshold intensity for optical field ionization on electron acceleration and propagation of intense laser pulse in plasma," *Japanese Journal of Applied Physics*, vol. 49, no. 9R, p. 096401, 2010. [Online]. Available: http://stacks.iop.org/1347-4065/49/i=9R/a=096401

[74] K.-G. Dong, Y.-C. Wu, B. Zhu, Y.-L. He, W.-M. Zhou, L.-F. Cao, H.-J. Liu, Z.-Q. Zhao, X.-L. Wen, C.-Y. Jiao, W. Hong, Y.-Q. Gu, B.-H. Zhang, and X.-F. Wang, "The influence of plasma density decreasement by pre-pulse on the laser wakefield acceleration," *AIP Advances*, vol. 1, no. 4, 2011. [Online]. Available: http://scitation.aip.org/content/aip/journal/adva/1/4/10.1063/1.3666041

[75] S. P. D. Mangles, A. G. R. Thomas, M. C. Kaluza, O. Lundh, F. Lindau, A. Persson, Z. Najmudin, C.-G. Wahlström, C. D. Murphy, C. Kamperidis, K. L. Lancaster, E. Divall, and K. Krushelnick, "Effect of laser contrast ratio on electron beam stability in laser wakefield acceleration experiments," *Plasma Physics and Controlled Fusion*, vol. 48, no. 12B, p. B83, 2006. [Online]. Available: http://stacks.iop.org/0741-3335/48/i=12B/a=S08

[76] T. Hosokai, K. Kinoshita, T. Ohkubo, A. Maekawa, M. Uesaka, A. Zhidkov, A. Yamazaki, H. Kotaki, M. Kando, K. Nakajima, S. V. Bulanov, P. Tomassini, A. Giulietti, and D. Giulietti, "Observation of strong correlation between quasimonoenergetic electron beam generation by laser wakefield and laser guiding inside a preplasma cavity," *Physical Review E (Statistical, Nonlinear, and Soft Matter Physics)*, vol. 73, no. 3, p. 036407, 2006. [Online]. Available: http://link.aps.org/abstract/PRE/v73/e036407

[77] B. S. Rao, J. A. Chakera, P. A. Naik, M. Kumar, and P. D. Gupta, "Laser wake-field acceleration in pre-formed plasma channel created by pre-pulse pedestal of terawatt laser pulse," *Physics of Plasmas*, vol. 18, no. 9, p. 093104, 2011. [Online]. Available: http://dx.doi.org/10.1063/1.3629983

[78] T. Hosokai, K. Kinoshita, A. Zhidkov, K. Nakamura, T. Watanabe, T. Ueda, H. Kotaki, M. Kando, K. Nakajima, and M. Uesaka, "Effect of a laser prepulse on a narrow-cone ejection of mev electrons from a gas jet irradiated by an ultrashort laser pulse," *Phys. Rev. E*, vol. 67, p. 036407, Mar 2003. [Online]. Available: http://link.aps.org/doi/10.1103/PhysRevE.67.036407

[79] T. Hosokai, K. Kinoshita, A. Zhidkov, K. Nakamura, H. Kotaki, M. Kando, K. Nakajima, and M. Uesaka, "Refraction effects on the cavity formation and interaction of an intense ultra-short laser pulse with a gas jet," *Phys. Plasmas*, vol. 11, no. 10, pp. L57–L60, 2004. [Online]. Available: http://link.aip.org/link/?PHP/11/L57/1

[80] C. G. Durfee and H. M. Milchberg, "Light pipe for high intensity laser pulses," *Phys. Rev. Lett.*, vol. 71, pp. 2409–2412, Oct 1993. [Online]. Available: https://link.aps.org/doi/10.1103/PhysRevLett.71.2409

[81] P. Volfbeyn, E. Esarey, and W. P. Leemans, "Guiding of laser pulses in plasma channels created by the ignitor-heater technique," *Phys. Plasmas*, vol. 6, no. 5, pp. 2269–2277, 1999. [Online]. Available: http://link.aip.org/link/?PHP/6/2269/1

[82] National photocolor. [Online]. Available: www.nationalphotocolor.com

[83] D. N. Fittinghoff, B. C. Walker, J. A. Squier, C. S. Toth, C. Rose-Petruck, and C. P. J. Barty, "Dispersion considerations in ultrafast cpa systems," *IEEE Journal of Selected Topics in Quantum Electronics*, vol. 4, no. 2, pp. 430–440, Mar 1998.

[84] S. Backus, C. G. Durfee, M. M. Murnane, and H. C. Kapteyn, "High power ultrafast lasers," *Review of Scientific Instruments*, vol. 69, no. 3, pp. 1207–1223, 1998. [Online]. Available: http://scitation.aip.org/content/aip/journal/rsi/69/3/10.1063/1.1148795

[85] B. C. Walker, C. Tóth, D. Fittinghoff, and T. Guo, "Theoretical and experimental spectral phase error analysis for pulsed laser fields," *J. Opt. Soc. Am. B*, vol. 16, no. 8, pp. 1292–1299, Aug 1999. [Online]. Available: http://josab.osa.org/abstract.cfm?URI=josab-16-8-1292

[86] A. Giulietti, P. Tomassini, M. Galimberti, D. Giulietti, L. A. Gizzi, P. Koester, L. Labate, T. Ceccotti, P. D'Oliveira, T. Auguste, P. Monot, and P. Martin, "Prepulse effect on intense femtosecond laser pulse propagation in gas," *Physics of Plasmas*, vol. 13, no. 9, 2006. [Online]. Available: http://scitation.aip.org/content/aip/journal/pop/13/9/10.1063/1.2351961

[87] W. P. Leemans, P. Catravas, E. Esarey, C. G. R. Geddes, C. Toth, R. Trines, C. B. Schroeder, B. A. Shadwick, J. van Tilborg, and J. Faure, "Electron-yield enhancement in a laser-wakefield accelerator driven by asymmetric laser pulses," *Phys. Rev. Lett.*, vol. 89, p. 174802, Oct 2002. [Online]. Available: https://link.aps.org/doi/10.1103/PhysRevLett.89.174802

[88] S. Steinke, J. van Tilborg, C. Benedetti, C. G. R. Geddes, C. B. Schroeder, J. Daniels, K. K. Swanson, A. J. Gonsalves, K. Nakamura, N. H. Matlis, B. H. Shaw, E. Esarey, and W. P. Leemans, "Multistage coupling of independent laser-plasma accelerators," *Nature*, vol. 530, no. 7589, pp. 190–193, 02 2016. [Online]. Available: http://dx.doi.org/10.1038/nature16525

[89] C. Tóth, J. Faure, J. van Tilborg, C. G. R. Geddes, C. B. Schroeder, E. Esarey, and W. P. Leemans, "Tuning of laser pulse shapes in grating-based compressors for optimal electron acceleration in plasmas," *Opt. Lett.*, vol. 28, no. 19, pp. 1823–1825, Oct 2003. [Online]. Available: http://ol.osa.org/abstract.cfm?URI=ol-28-19-1823

[90] K. Nakamura, H.-S. Mao, A. J. Gonsalves, A. Magana, J. Riley, C. Toth, and W. P. Leemans, "Diagnostics and controls for temporal structure of the bella laser system," *AIP Conference Proceedings*, vol. 1777, no. 1, p. 110004, 2016. [Online]. Available: http://aip.scitation.org/doi/abs/10.1063/1.4965693

[91] D. Zimmer, D. Ros, O. Guilbaud, J. Habib, S. Kazamias, B. Zielbauer, V. Bagnoud, B. Ecker, D. C. Hochhaus, B. Aurand, P. Neumayer, and T. Kuehl, "Short-wavelength soft-x-ray laser pumped in double-pulse single-beam non-normal incidence," *Phys. Rev. A*, vol. 82, p. 013803, Jul 2010. [Online]. Available: http://link.aps.org/doi/10.1103/PhysRevA.82.013803

[92] H. Vincenti and F. Quéré, "Attosecond lighthouses: How to use spatiotemporally coupled light fields to generate isolated attosecond pulses," *Phys. Rev. Lett.*, vol. 108, p. 113904, Mar 2012. [Online]. Available: http://link.aps.org/doi/10.1103/PhysRevLett.108.113904

[93] G. Zhu, J. van Howe, M. Durst, W. Zipfel, and C. Xu, "Simultaneous spatial and temporal focusing of femtosecond pulses," *Opt. Express*, vol. 13, no. 6, pp. 2153–2159, Mar 2005. [Online]. Available: http://www.opticsexpress.org/abstract.cfm?URI=oe-13-6-2153

[94] E. Block, J. Thomas, C. Durfee, and J. Squier, "Integrated single grating compressor for variable pulse front tilt in simultaneously spatially and

temporally focused systems," *Opt. Lett.*, vol. 39, no. 24, pp. 6915–6918, Dec 2014. [Online]. Available: http://ol.osa.org/abstract.cfm?URI=ol-39-24-6915

[95] D. N. Vitek, D. E. Adams, A. Johnson, P. S. Tsai, S. Backus, C. G. Durfee, D. Kleinfeld, and J. A. Squier, "Temporally focused femtosecond laser pulses for low numerical aperture micromachining through optically transparent materials," *Opt. Express*, vol. 18, no. 17, pp. 18 086–18 094, Aug 2010. [Online]. Available: http://www.opticsexpress.org/abstract.cfm?URI=oe-18-17-18086

[96] J. H. Odhner, K. M. Tibbetts, B. Tangeysh, B. B. Wayland, and R. J. Levis, "Mechanism of improved au nanoparticle size distributions using simultaneous spatial and temporal focusing for femtosecond laser irradiation of aqueous kaucl4," *The Journal of Physical Chemistry C*, vol. 118, no. 41, pp. 23 986–23 995, 2014. [Online]. Available: http://dx.doi.org/10.1021/jp507873n

[97] R. Trebino, P. Bowlan, P. Gabolde, X. Gu, S. Akturk, and M. Kimmel, "Simple devices for measuring complex ultrashort pulses," *Laser & Photonics Reviews*, vol. 3, no. 3, pp. 314–342, 2009. [Online]. Available: http://dx.doi.org/10.1002/lpor.200810032

[98] P. Gabolde and R. Trebino, "Single-shot measurement of the full spatio-temporal field of ultrashort pulses with multi-spectral digital holography," *Opt. Express*, vol. 14, no. 23, pp. 11 460–11 467, Nov 2006. [Online]. Available: http://www.opticsexpress.org/abstract.cfm?URI=oe-14-23-11460

[99] A. S. Wyatt, I. A. Walmsley, G. Stibenz, and G. Steinmeyer, "Sub-10 fs pulse characterization using spatially encoded arrangement for spectral phase interferometry for direct electric field reconstruction," *Opt. Lett.*, vol. 31, no. 12, pp. 1914–1916, Jun 2006. [Online]. Available: http://ol.osa.org/abstract.cfm?URI=ol-31-12-1914

[100] P. Bowlan, P. Gabolde, and R. Trebino, "Directly measuring the spatio-temporal electric field of focusing ultrashort pulses," *Opt. Express*, vol. 15, no. 16, pp. 10 219–10 230, Aug 2007. [Online]. Available: http://www.opticsexpress.org/abstract.cfm?URI=oe-15-16-10219

[101] F. Bragheri, D. Faccio, F. Bonaretti, A. Lotti, M. Clerici, O. Jedrkiewicz, C. Liberale, S. Henin, L. Tartara, V. Degiorgio, and P. D. Trapani, "Complete retrieval of the field of ultrashort optical pulses using the angle-frequency spectrum," *Opt. Lett.*, vol. 33, no. 24, pp. 2952–2954, Dec 2008. [Online]. Available: http://ol.osa.org/abstract.cfm?URI=ol-33-24-2952

[102] S. L. Cousin, J. M. Bueno, N. Forget, D. R. Austin, and J. Biegert, "Three-dimensional spatiotemporal pulse characterization with an acousto-optic pulse shaper and a hartmann–shack wavefront sensor," *Opt. Lett.*, vol. 37, no. 15, pp. 3291–3293, Aug 2012. [Online]. Available: http://ol.osa.org/abstract.cfm?URI=ol-37-15-3291

[103] F. Eilenberger, A. Brown, S. Minardi, and T. Pertsch, "Imaging cross-correlation frog: measuring ultrashort, complex, spatiotemporal fields," *Opt. Express*, vol. 21, no. 22, pp. 25 968–25 976, Nov 2013. [Online]. Available: http://www.opticsexpress.org/abstract.cfm?URI=oe-21-22-25968

[104] V. Gallet, S. Kahaly, O. Gobert, and F. Quéré, "Dual spectral-band interferometry for spatio-temporal characterization of high-power femtosecond lasers," *Opt. Lett.*, vol. 39, no. 16, pp. 4687–4690, Aug 2014. [Online]. Available: http://ol.osa.org/abstract.cfm?URI=ol-39-16-4687

[105] S. Akturk, X. Gu, P. Gabolde, and R. Trebino, "The general theory of first-order spatio-temporal distortions of gaussian pulses and beams," *Opt. Express*, vol. 13, no. 21, pp. 8642–8661, Oct 2005. [Online]. Available: http://www.opticsexpress.org/abstract.cfm?URI=oe-13-21-8642

[106] K. Nakamura, H. Vincenti, D. E. Mittelberger, H.-S. Mao, A. J. Gonsalves, C. Toth, and W. P. Leemans, "Diagnostics and controls for spatiotemporal couplings for laser-plasma accelerator drivers," *AIP Conference Proceedings*, vol. 1812, no. 1, p. 110008, 2017. [Online]. Available: http://aip.scitation.org/doi/abs/10.1063/1.4975921

[107] Z. Bor, B. Racz, G. Szabo, M. Hilbert, and H. A. Hazim, "Femtosecond pulse front tilt caused by angular dispersion," *Optical Engineering*, vol. 32, no. 10, pp. 2501–2504, 1993. [Online]. Available: http://dx.doi.org/10.1117/12.145393

[108] S. Akturk, M. Kimmel, P. O'Shea, and R. Trebino, "Measuring pulse-front tilt in ultrashort pulses using grenouille," *Opt. Express*, vol. 11, no. 5, pp. 491–501, Mar 2003. [Online]. Available: http://www.opticsexpress.org/abstract.cfm?URI=oe-11-5-491

[109] S. Akturk, X. Gu, E. Zeek, and R. Trebino, "Pulse-front tilt caused by spatial and temporal chirp," *Opt. Express*, vol. 12, no. 19, pp. 4399–4410, Sep 2004. [Online]. Available: http://www.opticsexpress.org/abstract.cfm?URI=oe-12-19-4399

[110] K. Varjú, A. P. Kovács, K. Osvay, and G. Kurdi, "Angular dispersion of femtosecond pulses in a gaussian beam," *Opt. Lett.*, vol. 27, no. 22, pp. 2034–2036, Nov 2002. [Online]. Available: http://ol.osa.org/abstract.cfm?URI=ol-27-22-2034

[111] C. G. Durfee, M. Greco, E. Block, D. Vitek, and J. A. Squier, "Intuitive analysis of space-time focusing with double-abcd calculation," *Opt. Express*, vol. 20, no. 13, pp. 14 244–14 259, Jun 2012. [Online]. Available: http://www.opticsexpress.org/abstract.cfm?URI=oe-20-13-14244

[112] S. Akturk, M. Kimmel, P. O'Shea, and R. Trebino, "Measuring spatial chirp in ultrashort pulses using single-shot frequency-resolved optical gating," *Opt. Express*, vol. 11, no. 1, pp. 68–78, Jan 2003. [Online]. Available: http://www.opticsexpress.org/abstract.cfm?URI=oe-11-1-68

[113] H. P. Vincenti, "Generation d'impulsions attosecondes sur miroir plasma relativiste," Ph.D. dissertation, Ecole Polytechnique X, 2013. [Online]. Available: https://pastel.archives-ouvertes.fr/pastel-00787281

Kei Nakamura (M'07) received the B.S. degree in electronic and information engineering from Tokyo Metropolitan University in 2000 and the M.S. and Ph.D. degrees in quantum engineering and system science from the University of Tokyo in 2002 and 2008 respectively. He joined LOASIS Program (currently BELLA Center) at the Lawrence Berkeley National Laboratory (LBNL) in 2004 for his Ph.D. work. He was a Postdoctoral Scholar at University of Nevada, Reno in 2008 and a Postdoctoral Scholar at LBNL from 2009 to 2012. Since 2013, he has been an Applied Physicist at LBNL.

His research interest includes intense laser-plasma interactions, high power ultrafast lasers and their diagnostics, magnetic optics for charged particle accelerators, and relativistic electron beam diagnostics. He received the Particle Accelerator Society of Japan Young Scientist Award for outstanding dissertation in 2008.

Hann-Shin Mao received his B.S., M.S., and Ph.D. degrees in aerospace engineering from the University of California, Los Angeles, with a concentration in fluid dynamics and plasma physics. Here, he studied miniature plasma sources for precision spacecraft propulsion for applications such as formation flying, disturbance compensation and attitude control. During his doctoral studies, he was a NASA graduate student research fellow at the Jet Propulsion Laboratory. Since 2013, he has been a postdoctoral research at the BELLA Center studying laser plasma accelerators. His main research interests include studying and developing specialized targets for various laser plasma accelerator applications.

Anthony J. Gonsalves (M'07) received his M.Sci. degree in Physics from the University of Bristol, UK, in 2000, and a Ph.D. in the Department of Physics, University of Oxford, UK, in 2006. He joined the LOASIS program (now named the BELLA center) in 2006 as a post-doctoral researcher in 2006, where he is currently a staff scientist. He is the head of plasma sources and control systems, and lead on the multi-GeV acceleration experiments performed with the BELLA peta-watt laser system. His research interests include high-intensity laser-plasma plasma interactions (e.g. for charged particle acceleration and radiation generation) and plasma waveguides.

Henri Vincenti is a Marie Curie Fellow at the Lawrence Berkeley National Laboratory and Commissariat a l'Energie Atomique (CEA) in France. His research interests include high performance computing and data structure optimization for future exascale computers, ultra high-order/pseudo-spectral numerical methods for solving Maxwell's equations, as well as numerical/theoretical study with electromagnetic Particle-In-Cell (PIC) codes of laser plasma interactions at ultrahigh intensity with plasmas including high-order harmonic/electron/ion production on relativistic plasma mirrors. Vincenti holds a MSc. in Electrical Engineering and Computer Science from SUPELEC (France), a MSc. in Nuclear Fusion from Ecole Polytechnique (France) and a PhD in theoretical/computational physics from Ecole Polytechnique (France).

Daniel E. Mittelberger received his B.S. in physics and B.A. in mathematics from the George Washington University in Washington, DC, in 2007 and his M.A. in physics from the University of California, Berkeley, in 2010. He is currently pursuing a Ph.D. in physics at the University of California, Berkeley.

From 2005 to 2007, he was a Research Assistant with the nuclear physics group at the George Washington University. In 2008, he worked as a Student Guest Researcher at the 88 inch Cyclotron at LBNL. He joined the BELLA Center at LBNL in 2010 for his Ph.D. research where he studies laser plasma acceleration. His research interests include high-intensity-laser plasma interactions, ultrafast laser pulse characterization, and iterative reconstruction such as phase retrieval techniques.

Joost Daniels received the B.S. and M.S. degree in applied physics at Eindhoven University of Technology (TU/e) in Eindhoven, The Netherlands, specializing in the disciplines of Sustainable Energy Technology and Plasma & Radiation. As part of his Master's program, he did an internship at the Dutch Institute for Fundamental Matter Research (DIFFER) studying plasma-surface interactions for fusion reactors, and worked on laser-plasma accelerators at Lawrence Berkeley National Laboratory (LBNL) in Berkeley, USA. He is currently pursuing the Ph.D. degree through Eindhoven University, by continuing his work at the BELLA Center at LBNL, developing and applying novel diagnostic techniques and controls involving plasma channels for high-power lasers and particle acceleration.

Arturo Magana earned an Associates Degree from DeVry Institute of Technology, Phoenix, Arizona in 1983. With more than 25 years of experience working for various renowned laser companies such as Spectra-Physics, Quantel Lasers, Positive Light and Coherent Inc, he has progressively worked his way from manufacturing technician, to final test supervisor, service engineer as well as research & development engineer.

While at Lawrence Berkeley National Laboratory, he was part of the BELLA team that broke the world record using a laser-plasma based accelerator generating 4.25 GeV electron beams. He continues to support the BELLA laser Peta-watt system assisting scientists in their efforts towards producing 10 GeV electron beams.

Csaba Toth received his M.Sc. and Ph.D. degrees in Laser Physics and Quantumelectronics from the Etvs University, Budapest, Hungary in 1983 and 1987, respectively. He started his scientific activity in the Research Institute for Solid State Physics, Budapest, Hungary, followed by numerous international collaborations in various laser laboratories in Europe. In 1993 and from 1995-97 he was a visiting scholar at Rice University, Houston, TX, then from 1997 till 2000 he was a project scientist in the Institute for Nonlinear Science and The Wilson Group of the University of California at San Diego, CA. In November 2000 he joined the Lawrence Berkeley National Laboratory (LBNL), Berkeley, California as a staff physicist, where he was responsible for the laser systems and experimental activities of the l'OASIS (Lasers, Optical Accelerators System Integrated Studies) Group. This group by 2014 evolved to the BELLA Center, where he is now Staff Scientists and Operations Coordinator. Dr. Toth's research interests include the interactions of ultrashort, high intensity light pulses with matter: multiphoton processes, optical tunneling, higher-order optical harmonic generation, laser-plasma interactions, acceleration of electrons and other charged particles by high peak-power laser pulses and plasma waves, development and application of new X-ray sources for imaging, time-resolved diffraction, and absorption at ultrafast time scales. He has published more than 160 papers; these papers have been cited over 8500 times. His honors include the Soros Fellowship for Young Scientists of Hungary (1990), the Jnossy Award of the Central Research Institute for Physics, Budapest (1990), the John Dawson Award for Excellence in Plasma Physics Research by APS (2010), and the Department of Energy Secretary's Achievement Award (2014). Dr. Csaba Toth is a member of the Optical Society of America (OSA), the Hungarian, American and European Physical Societies (ELFT, APS, EPS).

Wim P. Leemans (M'87–F'07) is Director of the Accelerator Technology and Applied Physics Division at Lawrence Berkeley National Laboratory (LBNL). After earning a Ph.D. in electrical engineering in 1991 from UCLA, he immediately joined LBNL. He started the LOASIS Program in 1994 (now named the BELLA Center), which he continues to lead. His personal research interest is in advanced accelerator and radiation source concepts and their applications. He has over 370 publications and more than 9,700 citations, two patents, and has served on many panels and committees, including the 2014 P5 that developed the U.S. strategic plan for high energy physics. He also organized multiple workshops that have led to the development of community-based input to national and international roadmaps for advanced accelerator technology.

He has received several prestigious awards, including the 2005 USPAS Prize for Achievement in Accelerator Physics and Technology, the 2009 E.O. Lawrence Award from DOE, the 2010 APS J.M. Dawson Award for Excellence in Plasma Physics Research, the 2012 Advanced Accelerator Concepts Prize, the 2013 DOE Secretary's Achievement Award for the BELLA Project, and the 2016 IEEE Particle Accelerator Science and Technology (PAST) award. He is a Fellow of APS, IEEE and AAAS.

He has been research advisor for more than twenty PhD graduate students, two of whom received the APS outstanding dissertation award (2005 & 2006) and one of whom received the Japanese PASJ prize for outstanding dissertation (2008).